NASA/CR—2009-215498

Long Term Measurement of the Vapor Pressure of Gold in the Au–C System

Evan H. Copland
Case Western Reserve University, Cleveland, Ohio

July 2009

NASA STI Program . . . in Profile

Since its founding, NASA has been dedicated to the advancement of aeronautics and space science. The NASA Scientific and Technical Information (STI) program plays a key part in helping NASA maintain this important role.

The NASA STI Program operates under the auspices of the Agency Chief Information Officer. It collects, organizes, provides for archiving, and disseminates NASA's STI. The NASA STI program provides access to the NASA Aeronautics and Space Database and its public interface, the NASA Technical Reports Server, thus providing one of the largest collections of aeronautical and space science STI in the world. Results are published in both non-NASA channels and by NASA in the NASA STI Report Series, which includes the following report types:

- TECHNICAL PUBLICATION. Reports of completed research or a major significant phase of research that present the results of NASA programs and include extensive data or theoretical analysis. Includes compilations of significant scientific and technical data and information deemed to be of continuing reference value. NASA counterpart of peer-reviewed formal professional papers but has less stringent limitations on manuscript length and extent of graphic presentations.

- TECHNICAL MEMORANDUM. Scientific and technical findings that are preliminary or of specialized interest, e.g., quick release reports, working papers, and bibliographies that contain minimal annotation. Does not contain extensive analysis.

- CONTRACTOR REPORT. Scientific and technical findings by NASA-sponsored contractors and grantees.

- CONFERENCE PUBLICATION. Collected papers from scientific and technical conferences, symposia, seminars, or other meetings sponsored or cosponsored by NASA.

- SPECIAL PUBLICATION. Scientific, technical, or historical information from NASA programs, projects, and missions, often concerned with subjects having substantial public interest.

- TECHNICAL TRANSLATION. English-language translations of foreign scientific and technical material pertinent to NASA's mission.

Specialized services also include creating custom thesauri, building customized databases, organizing and publishing research results.

For more information about the NASA STI program, see the following:

- Access the NASA STI program home page at *http://www.sti.nasa.gov*

- E-mail your question via the Internet to *help@sti.nasa.gov*

- Fax your question to the NASA STI Help Desk at 443–757–5803

- Telephone the NASA STI Help Desk at 443–757–5802

- Write to:
  NASA Center for AeroSpace Information (CASI)
  7115 Standard Drive
  Hanover, MD 21076–1320

NASA/CR—2009-215498

Long Term Measurement of the Vapor Pressure of Gold in the Au–C System

Evan H. Copland
Case Western Reserve University, Cleveland, Ohio

Prepared under Contract NNC07BA13B

National Aeronautics and
Space Administration

Glenn Research Center
Cleveland, Ohio 44135

July 2009

Level of Review: This material has been technically reviewed by NASA technical management.

Available from

NASA Center for Aerospace Information
7115 Standard Drive
Hanover, MD 21076–1320

National Technical Information Service
5285 Port Royal Road
Springfield, VA 22161

Available electronically at http://gltrs.grc.nasa.gov

Long Term Measurement of the Vapor Pressure of Gold in the Au–C System

Evan H. Copland
Case Western Reserve University
Cleveland, Ohio 44106

Abstract

Incorporating the {Au(s,l) + graphite} reference in component activity measurements made with the multiple effusion-cell vapor source mass spectrometry (multicell KEMS) technique provides a fixed temperature defining ITS-90 (T_{mp}(Au) = 1337.33K) and a systematic method to check accuracy. Over a 2 year period ΔH_{sub}(298)Au was determined by the 2nd and 3rd law methods in 25 separate experiments and were in the ranges 362.2±3.3 kJmol^{-1} and 367.8±1.1 kJmol^{-1}, respectively. This ~5 kJmol^{-1} discrepancy is transferred directly to the measured activities. This is unacceptable and the source of this discrepancy needs to be understood and corrected. Accepting the 2nd law value increases p(Au) by about 50%, brings the 2nd and 3rd law values into agreement and removes the T dependence in the 3rd law values. While compelling, there is no way to independently determine instrument sensitivities, S_{Au}, with T in a single experiment with *KEMS*. This lack of capability is stopping a deeper understanding of this problem. In addition, the Au–C phase diagram suggests a eutectic invariant reaction: L-Au(4.7at%C) = *FCC*-Au(0.08at%C) + C(graphite) at T_e~1323K. This high C concentration in Au(l) must reduce p(Au) in equilibrium with {Au(s,l) + graphite} and raises some critical questions about the Gibbs free energy functions of Au(s,l) and the Au fixed point (T_{mp}(Au) = 1337.33K) which is always measured in graphite.

1. Introduction

Multiple Knudsen effusion-cell mass spectrometry, multicell KEMS, is an important technique for studying the partial thermodynamic properties of vapor and condensed phases and reactions involving vapor species at high temperatures [ING1959, DRO2005]. Partial thermodynamic properties or component activities, a(i), provide direct information about the shape of Gibbs energy surfaces of phases in multicomponent alloy and ceramic systems and are also a powerful tool to study complex phase transformations [COP2007]. Accurate Gibbs energy and phase equilibrium data are critical to ensure that thermodynamic descriptions found in computational thermodynamic models accurately represent the behavior of real materials [SAU1998]. Activities are determined with KEMS by the "vapor pressure" method by comparing the partial pressure of a characteristic vapor species, p(i), in equilibrium with an alloy sample to its partial pressure in equilibrium with a condensed reference state, $p°$(i), according to the definition of activity: $a(\mathrm{i}) = p(\mathrm{i})/p°(\mathrm{i})$ [LEW1961, LUP1983]. The effusion cell allows the vapor to approach equilibrium while p(i) is sampled by effusion and the relative partial pressure are determined from the measured ion intensity of a representative ion beam, I_i, and absolute temperature, T, according to: $p(\mathrm{i}) = I_i T/S_i$ (where S_i is the instrument sensitivity: cpsKatm^{-1}) [ING1959]. Absolute partial pressure measurements require that S_i is known and remains stable over multiple experiments [HIL1996]. In practice, it is hard to calculate and measure accurate S_i values for KEMS measurements [DRO2005]. The requirements for S_i are removed, to a large degree, with a multiple effusion-cell vapor source or multicell KEMS instrument [BUC1966, CHA1974~2002], which allows the relative partial pressure of species in equilibrium with different condensed samples, in adjacent effusion-cells, to be determined directly. The multicell KEMS instrument used in this study has 3 isothermal effusion-cells and molecular beam sampling is independent of the effusion orifice [CHA1974~2002, COP2006]. Ideally the alloy and pure element reference are placed in adjacent effusion-cells and activities are determined directly, $a(\mathrm{i}) = I_i/I°_i$ [BUC1966, CHA1974~2002], but this is usually impractical because $p°$(i) is too high (>10^{-4} atm) and pure elements are too reactive (*e.g.*, pure-Al(l)). An indirect procedure using {Au(s,l) + graphite} as a secondary reference, equation (1), turns out to be more practical, but more complicated.

$$a(\mathrm{i}) = \left.\frac{p(\mathrm{i})}{p^\circ(\mathrm{Au})}\right|_T \cdot \left[\left.\frac{p^\circ(\mathrm{Au})}{p^\circ(\mathrm{i})}\right|_T\right] = \left.\frac{I_\mathrm{i}}{I^\circ_\mathrm{Au}}\right|_T \cdot \frac{S_\mathrm{Au}}{S_\mathrm{i}} \cdot \frac{g_\mathrm{Au}}{g_\mathrm{alloy}} \cdot \left[\left.\frac{p^\circ(\mathrm{Au})}{p^\circ(\mathrm{i})}\right|_T\right] \tag{1}$$

Activities are determined at each T by comparing the measured ratio $p(i)/p°(Au)$ or $I_i/I°_{Au}$, to the accepted evaporation behavior $[p°(Au)/p°(i)]$ of {Au(s,l) + graphite} and the pure-element reference. The g_{Au}/g_{alloy} term accounts for variations in effusion-orifices and are routinely measured to be 1.00±0.01 for a pair of cells [COP2007, COP2005]. The S_{Au}/S_i term is an instrument sensitivity (or ionization cross-section) ratio that relates the secondary reference, {Au(s,l) + graphite}, $p°(Au)$, to the pure-element reference, $p°(i)$, and they are determined in a separate experiment comparing measured ratio of the evaporation behavior of and the pure-element reference/{Au(s,l) + graphite}, $I°_{Au}/I°_i$, to the accepted evaporation behavior $[p°(i)/p°(Au)]$. The S_{Au}/S_i terms must be independent of T, thus the accepted evaporation behavior for both must be correct and able to be measured routinely [COP2007, COP2005].

$$\frac{S_{Au}}{S_i} = \frac{I^o_{Au}}{I^\circ_i}\bigg|_T \cdot \frac{g_i}{g_{Au}} \cdot \left[\frac{p^\circ(i)}{p^\circ(Au)}\bigg|_T\right] \qquad (2)$$

This procedure provides the following advantages: 1) two alloys can be measured in a single experiment; 2) T measurement are calibrated with by melting Au in each experiment ($T_{mp}(Au) = 1337.33K$ is a fixed point defining ITS-90) [McG1990, PRE1990]; 3) routine measurements of the evaporation enthalpy of Au, $\Delta H_{sub}(298.15)Au$, by the 2nd and 3rd law methods provide a systematic accuracy check [PAU1970a]. This procedure was used to measure a(Al) and a(Ni) at more then 30 alloy compositions in the Ni-rich corner of the Ni-Al-Pt(-O) system, some of this data are found in references [COP2007, COP2006, COP2005]. Reviewing this data raises some critical questions about the accepted vapor pressure of Au, our knowledge of the Au–C system and provides direction for the future development of the KEMS technique.

2. Experimental and Results

In all experiments 1.5 to 2.5 gm of high purity Au (99.999wt%, Alfa Aesar, premion) were placed in either a graphite or a graphite lined Al_2O_3 effusion-cell. To limit contamination from matter effusing into the effusion-cell from the furnace or reaction between the Al_2O_3 cell and graphite liner, an Au sample was never used for more then 3 consecutive experiments. Evidence of contamination was checked periodically, and total contamination was always less then 200 ppm. The effusion cells had 1.5 mm diameter x 4.0 mm orifices and inner cell dimensions of 10 mm in diameter x 7 mm tall. Before use, the Al_2O_3 and graphite effusion cells were cleaned by soaking in acid (aqua-regia) and baking at about 1800 K for 10 hr under vacuum (~10^{-8} atm).

Temperature was determined by measuring the current of the detector, A, of a pyrometer (M190V–TS, *Mikron Infrared,* New Jersey) sighting a blackbody source (2.5 mm in diameter x 13.5 mm in each effusion-cell and Mo-cell holder) using the relationship: $1/T = a_0 + a_1\ln(A/e) + a_2(\ln(A/e))^2 + a_3(\ln(A/e))^3$. The a_i terms are the calibration of the pyrometer determined at 9 NIST traceable temperatures over the temperature range 1100 to 2500K. e is the "emissivity of the optic path" and is the combination of the blackbody source plus the transmissivity of the vacuum chamber window. The pyrometer calibration is assumed constant while e varies between experiments due to deposition of vapor species and subsequent cleaning of the vacuum chamber window. The onset of Au melting was identified by the arrest point in the measured T_{meas} vs. *time* plot (point A) together with the start of the plateau in the plot of I_{Au} vs. *time* plot, shown in figure 1(a). The value of e was determined in each experiment from the measured detector current at the melting temperature of Au ($T_{mp}(Au) = 1337.33$ K), this e value was then used to correct the measured temperature, $\Delta T = T_{meas} - T_{corr}$, over the whole temperature range considered in each experiment, as shown in figure 1(b). Au melting was usually measured two or more times in an experiment to check reproducibility, and after the initial calibration, $T_{mp}(Au)$ was determined to be 1337.0±0.5 K. The measured e and ΔT at Au melting in each experiment are listed in table 1 in columns 5 and 4, respectively. (The apparent inconsistencies in e values results from changing the window material from sapphire to quartz, also the experimental runs are not listed in chronological order.)

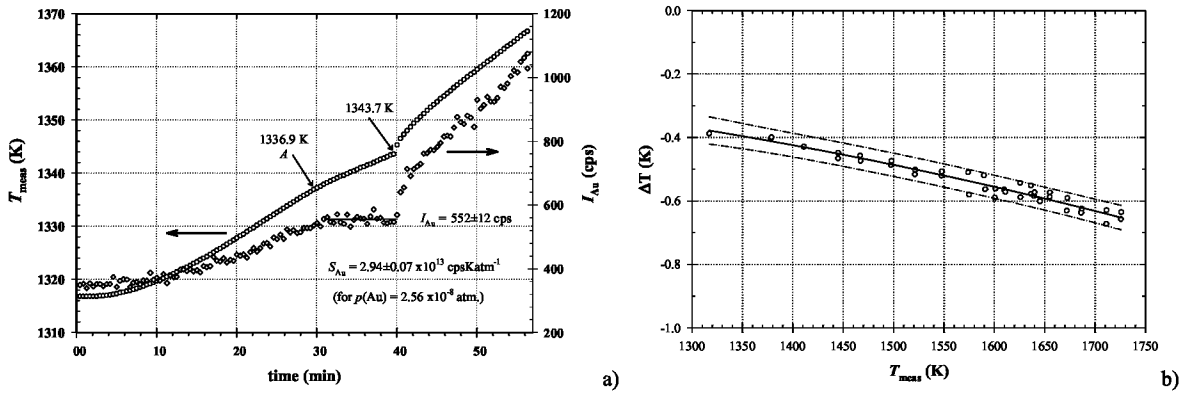

Figure 1.—a) Typical measured T_{meas} and I_{Au} vs. *time* plot made during run 1 as the furnace was ramped through the melting temperature of Au. The arrest in T vs. *time* plot (point A) signifies the onset of melting, while the plateau in the I_{Au} vs. *time* plot corresponds to a fixed p(Au) defined by the {Au(s) + Au(l) + Au(g) + C(s)} invariant in the Au–C system. b) Temperature correction, $\Delta T = T_{meas} - T_{corr}$, vs. T_{meas} over the temperature range considered in run 1.

The plateau in I_{Au} shows p(Au) and T are fixed inside the effusion-cell for 10~15 min while the {Au(s) + Au(l) + Au(g) + graphite} invariant exists. The plateau in T_{meas} is not observed because the furnace continued to ramp after the start of melting and the black body source is not fully surrounded by Au as with typical fixed-point black body sources [FIS1989]. The fixed p(Au) is identified as 2.56×10^{-8} atm in reference [PAU1970a], which was used to determine S_{Au}(3rd) in each experiment: $S_{Au}(3rd) = I_{Au}T/p(Au)$. These values are listed in column 9 of table 1 and were used to determine absolute p(Au) over the temperature range in each experiment, as shown for run 1 in figure 2(b). These pressures were used to determine the enthalpy of sublimation, $\Delta_{sub}H(298)$ of Au(s) by the 3rd law method using equation (3) and the procedure discussed in references [PAU1970, CHA1998]. The Gibbs free energy functions for condensed and vapor Au used in these calculations were a combination of the values reported in PAU1970 and GUR1993 and are listed in table A1 of the appendix. The 3rd law method gives $\Delta_{sub}H(298)$ at each temperature, but the average value for each experiment is listed in column 8 of table 1. $\Delta_{sub}H(298)$ of Au(s) was also determined at 298K by the 2nd law method with the least-squares fitting of coefficients A and B in equation (4).

$$T\left[\Delta\left\{-\left(G_T^o - H_{298}^o\right)/T\right\} - R\ln p(\mathrm{Au})\right] = \Delta H_{sub}(298.15)Au \tag{3}$$

$$\Delta\left\{-\left(G_T^o - H_{298}^o\right)/T\right\} - R\ln(I_{Au}T) = A + B/T \tag{4}$$

This calculation is similar to the sigma method [CUB1966, HOR1966] and the slope B gives the enthalpy of sublimation at $T = 298$K, as shown in figure 2(a). In the 2nd law calculation the instrument sensitivity S_{Au}(2nd) was assumed to be constant but the value determined at the {Au(s) + Au(l) + Au(g) + graphite} invariant was not used. The intercept coefficient, A, is equated to $-R\ln(S_{Au})$ and an estimate of S_{Au}(2nd) was obtained. Both the intercept A and S_{Au}(2nd) are listed column 7 of table 1. The discrepancy between S_{Au}(3rd) and S_{Au}(2nd) for an experiment represents the change in absolute p(Au) needed for the 2nd and 3rd law determinations of $\Delta_{sub}H(298)$ to agree. This change is given by the ratio $S_{Au}(3rd)/S_{Au}(2nd)$ listed in column 10 of table 1. The complete set of results from all 25 experiments are found in the appendix.

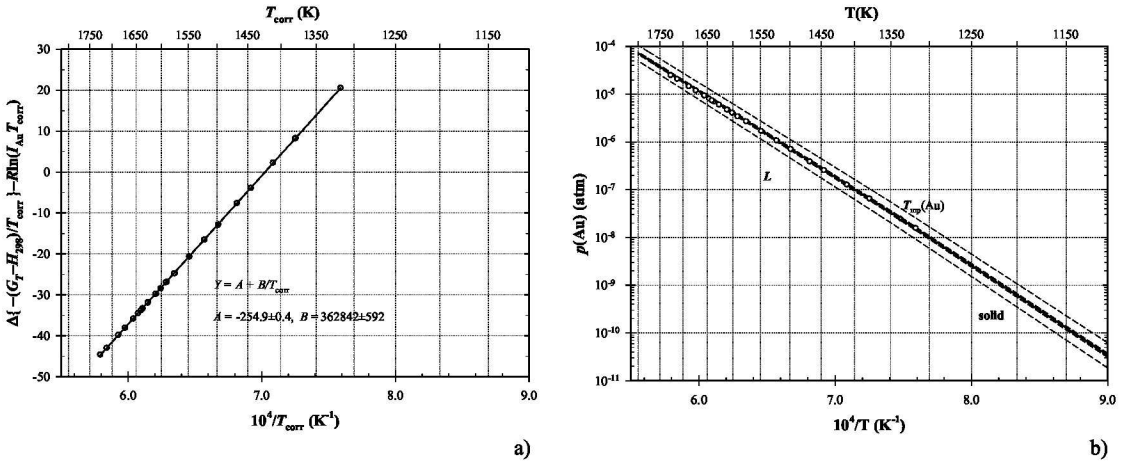

Figure 2.—Evaporation behavior of {Au(s,l) + graphite} determined during run 1. a) Second law determination of $\Delta H_{sub}(298.15)$Au (= 362.8±0.6 kJmol^{-1}) from least squares fit of $\Delta\{-(G°_T-H°_{298})/T\}-R\ln(I_{Au}T)$ vs. $1/T$. b) Measured p(Au) vs. $1/T$ compared to accepted evaporation behavior [PAU1970, GUR1993]. In addition to the central prediction (solid line) of the evaporation behavior of Au(s,l) for $\Delta H_{sub}(298.15)$Au = 367.0 kJmol^{-1}, this plot also shows the 95% confidence bands at the ±0.9 kJmol^{-1} and ±5.6 kJmol^{-1} levels (dashed lines).

Table 1.—Summary of Second and Third law Measurements of $\Delta H_{sub}(298)$ for {Au(s) + graphite}

run	#	T range (K)	ΔT at T_{mp}(Au)	"e"	slope B (kJmol^{-1})	intercept A (S_{Au}(2nd)) (cpsKatm^{-1})/10^{13}	$\Delta H_{sub}(298)$ (kJmol^{-1})	S_{Au}(3rd) (cpsKatm^{-1})/10^{13}	S_{Au}(3rd) / S_{Au}(2nd)
1	41	1317–1727	–0.43	1.038	362.8±0.6	–254.9±0.4 (2.07±0.09)	367.4±0.7	2.94±0.07	1.42
2	30	1317–1677	2.97	1.044	363.1±0.5	–255.2±0.3 (2.15±0.09)	368.3±0.7	3.2±0.1	1.50
3	26	1331–1762	–7.3	0.92	364.9±1.3	–255.6±0.9 (2.24±0.25)	368.4±0.9	2.93±0.07	1.31
4	43	1319–1745	–1.7	1.024	360.3±0.9	–249.3±0.6 (1.05±0.08)	368.3±1.2	1.92±0.04	1.83
5	31	1322–1733	–1.63	1.022	361.1±1.3	–252.4±0.9 (1.54±0.17)	367.9±1.3	2.6±0.9	1.68
6	19	1325–1749	–3.1	0.984	362.3±1.2	–249.2±0.9 (1.04±0.11)	368.3±1.1	1.63±0.05	1.57
7	33	1325–1751	–3.7	0.9961	360.9±1.0	–252.2±0.6 (1.49±0.12)	368.5±1.1	2.62±0.08	1.76
8	22	1322–1742	–1.7	1.021	362.7±1.2	–249.7±0.8 (1.10±0.11)	368.0±1.0	1.67±0.05	1.52
9	34	1332–1733	–4.8	0.982	362.8±2.7	–252.9±1.8 (1.6±0.4)	368.5±1.4	2.51±0.05	1.57
10	28	1320–1717	–0.73	1.0385	362.0±1.2	–249.8±0.8 (1.1±0.1)	367.7±1.0	1.73±0.03	1.57
11	34	1333–1730	–5.2	0.979	358.3±1.8	–248.2±1.2 (0.92±0.1)	368.3±1.7	1.96±0.07	2.13
12	28	1323–1739	–5.33	0.979	361.4±1.4	–250.5±1.0 (1.2±0.1)	368.0±1.2	2.02±0.05	1.68
13	29	1315–1745	–1.1	1.03	361.6±0.9	–251.6±0.7 (1.4±0.1)	367.6±0.9	2.19±0.05	1.57
14	32	1317–1747	–1.33	1.02	360.2±1.6	–251.0±1.1 (1.3±0.1)	368.2±1.2	2.35±0.05	1.81
15	35	1315–1708	–0.93	1.031	363.5±0.8	–256.6±0.6 (2.5±0.2)	367.3±0.6	3.36±0.07	1.34
16	34	1324–1688	–4.03	0.993	363.6±0.6	–251.2±0.4 (1.32±0.06)	367.3±0.6	1.75±0.05	1.33
17	38	1315–1732	–0.4	1.038	361.3±1.0	–253.2±0.7 (1.7±0.1)	367.6±0.9	2.69±0.09	1.58
18	39	1319–1724	–0.2	1.04	364.0±0.5	–256.6±0.3 (2.54±0.09)	367.5±0.5	3.32±0.05	1.31
19	20	1319–1629	–2.2	1.015	364.5±0.8	–254.6±0.5 (2.0±0.1)	367.2±0.4	2.44±0.05	1.22
20	19	1325–1623	–1.2	1.028	364.0±0.7	–254.2±0.5 (1.9±0.1)	367.2±0.4	2.45±0.07	1.29
21	44	1315–1715	–2.23	1.055	362.3±0.6	–253.2±0.4 (1.69±0.08)	368.0±0.8	2.62±0.08	1.55
22	21	1319–1637	–2.83	1.012	364.7±0.6	–254.8±0.4 (2.1±0.1)	366.9±0.3	2.44±0.07	1.16
23	9	1475–1630	–1.0	1.038	363.4±1.8	–251.5±1.2 (1.4±0.2)	367.4±0.4	1.90±0.07	1.29
24	38	1165–1514	–0.6	0.986	360.4±2.3	–261.6±1.9 (4.6±0.9)	366.6±1.4	8.14±0.2	1.77
25	35	1329–1674	–4.2	0.990	363.1±2.9	–264.8±2.0 (6.8±0.9)	367.4±1.1	9.5±0.2	1.40
					362.2±3.3		**367.8±1.1**		

Note experimental runs are not listed in chronological order.

3. Discussion

From the summary of results from all 25 experiments listed in table 1 the 3rd law $\Delta_{sub}H(298)Au$ (average for all 25 runs: 367.8±1.1 kJmol^{-1}) agrees with the accepted evaporation behavior of Au(s,l) while the values determined by the 2nd law (average for all 25 runs: 362.2±3.3 kJmol^{-1}) are typically 5 kJmol^{-1} lower. This level of discrepancy (~1.4%) between 2nd and 3rd law measurements is typically acceptable for evaporation studies, but in this case {Au(s,l) + graphite} is used as a secondary reference to determine component activities. This calculation, equation (1), is a relative partial pressure measurement that relies on the ability to consistently measure the accepted evaporation behavior of {Au(s,l) + graphite}. In this case the 2nd law values are the measured behavior while the 3rd law data represents the accepted behavior. Any discrepancy between the measured and accepted behavior of {Au(s,l) + graphite} and the pure-element reference is transferred directly to the measured a(i) and the observed solution behavior. In terms of Gibbs energy surfaces and multicomponent solution behavior a 5 kJmol^{-1} uncertainty is significant and will have a large affect on the predicted phase equilibrium in a system based on measured activities. The only way to remove this 5 kJmol^{-1} uncertainty from the a(i) values is to verify that the 2nd law $\Delta_{sub}H(298)Au$ is routinely reproduced and use this value to update the accepted evaporation behavior of {Au(s,l) + graphite} [COP2007, COP2005]. The justification, result of doing this and critical remaining questions are the focus of this discussion.

Calibrating the pyrometer with the Au melting point ensures T_{corr} reproduces the thermodynamic temperature scale (ITS-90) [PRE1990, McG1990] as accurately as possible over the temperature range considered in each experiment. T measurements are not expected to be a significant source of error in these experiments. In addition it is important to recognize that the same I_{Au} and T_{corr} measurements and Gibbs free energy functions are used in both 2nd and 3rd law calculations, therefore the observed difference between the two must result from either one or a combination of the following: 1) a discrepancy between p(Au) in equilibrium with {Au(s,l) + graphite} and free energy functions of Au, 2) an error in the free energy functions of Au, or 3) a temperature or count rate dependence in S_{Au}, unrelated to the evaporation of {Au(s,l) + graphite}.

As stated in section 2, the instrument sensitivity, S_{Au}(3rd), was determined at the {Au(s) + Au(l) + Au(g) + graphite} invariant by accepting that p(Au) = 2.56x10^{-8} atm. [PAU1970a]. This is the easiest way of determining S_{Au} and is ideal for a routine accuracy check when measuring activities. However, as it was then used to determine absolute p(Au) it forces the subsequent 3rd law calculations to fit the of the accepted evaporation behavior for Au. The fact that S_{Au}(3rd) was not determined independently of the expected evaporation behavior diminishes the significance of the 3rd law data. In contrast, the 2nd law calculation does not presume the evaporation behavior, but simply assumes S_{Au} remains constant during the course of an experiment (*i.e.*, independent of T, time and count rate). These more objective assumptions together with the similar level of uncertainty observed in the 2nd and 3rd law calculations in most experiments (table 1 and fig. 2(a)) suggest that the 2nd law values should be given more significance then they are normally given in this case. The most likely reason for the discrepancy between 2nd and 3rd law values is initially seen in fig. 2(b) where p(Au) falls below the expected behavior at high T. Identical behavior was seen in all 25 experiments as shown in figure 3(a) where measured p(Au) are compared to the expected behavior [PAU1970a] (and in appendix). In all cases p(Au) remains well within the ±5.6 kJmol^{-1} confidence band but drops bellow the ±0.9 kJmol^{-1} level at high T and rises above the ±0.9 kJmol^{-1} level at low T. A lower then the expected p(Au) corresponds to a high $\Delta_{sub}H(298)Au$ and a small T dependence was observed in the 3rd law calculations in each experiment, as shown in figure 3(b) and figure 4. This agrees with the lower $\Delta_{sub}H(298)Au$ values observed with the 2nd law calculations. Corresponding to the method used to determine S_{Au}(3rd), $\Delta_{sub}H(298)Au$ and p(Au) show the best agreement with the accepted behavior at the {Au(s) + Au(l) + Au(g) + graphite} invariant, but diverge at higher and lower T.

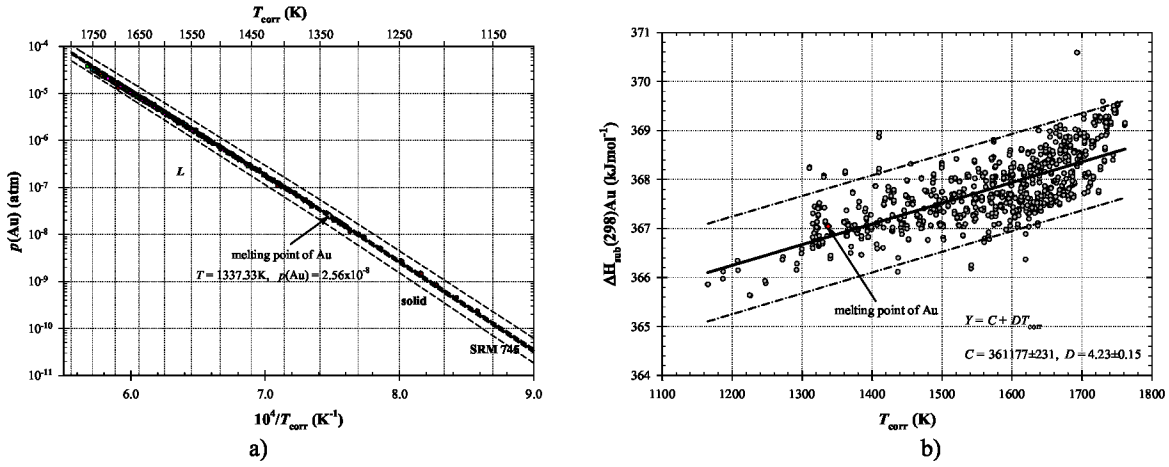

Figure 3.—a) All measured p(Au) from all 25 experiments plotted against $1/T_{corr}$ and compared to accepted evaporation behavior [PAU1970, GUR1993]. The central prediction (solid line) of the evaporation of Au(s,l) is based on $\Delta H_{sub}(298.15)Au = 367.0$ kJmol^{-1}. This plot also shows the 95% confidence bands at the ±0.9 kJmol^{-1} and ±5.6 kJmol^{-1} levels (dashed lines). b) Third law measurements of $\Delta H_{sub}(298.15)Au$ from all 25 experiments plotted against T_{corr}.

The most obvious reason for the T dependence of $\Delta_{sub}H(298)Au$ is p(Au) in equilibrium with {Au(s,l) + graphite} is higher then currently accepted. An estimate of how much higher can be obtained by comparing S_{Au}(3rd) to the estimate obtained from the intercept A of least squares fit in the 2nd law calculation ($A = -R\ln(S_{Au})$): $S_{Au}(3rd)/S_{Au}(2nd)$. For run 1, increasing p(Au) by about 42% brings both the 2nd and 3rd law values into agreement and removes the T dependence in $\Delta_{sub}H(298)Au$, as shown in figure 4.

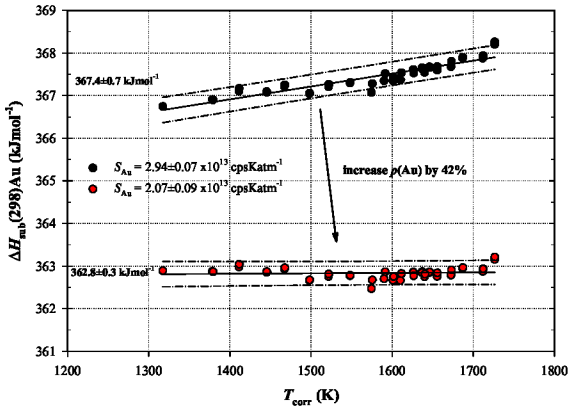

Figure 4.—Comparison of the 3rd law $\Delta H_{sub}(298.15)Au$ for run 1 for two p(Au) using S_{Au}(3rd) determined at the {Au(s) + Au(l) + Au(g) + graphite} invariant (2.94±0.07x10^{13} cpsKatm^{-1}) and from intercept A = –254.9±0.4 (S_{Au}(2nd) = 2.07±0.09x10^{13} cpsKatm^{-1}); $S_{Au}(3rd)/S_{Au}(2nd)$ = 1.42 or a 42% increase in p(Au).

The corresponding increase in p(Au) all experiments gave the same behavior as figure 4. On average this suggests that the accepted p(Au) in equilibrium with {Au(s,l) + graphite} should be increased by about 50%. Therefore, in addition to removing the 5 kJmol^{-1} discrepancy from the measured a(i), accepting the 2nd law value, $\Delta_{sub}H(298)Au = 362.2$ kJmol^{-1}, for the evaporation behavior of {Au(s,l) + graphite} effectively increase the p(Au) by 50% over the whole temperature range. However, the evidence for increasing p(Au) from these measurements is not irrefutable because the predicted in crease, $S_{Au}(3rd)/S_{Au}(2nd)$, ranges from 16 to 113% with an average value of 53±23%. If low p(Au) was the only factor involved a consistent $S_{Au}(3rd)/S_{Au}(2nd)$ and difference between the 2nd and 3rd law values should have being observed. While the variation shown in table 1 could be due to random error it opens the possibility that other factors may be influencing instrument sensitivity like: 1) thermal expansion of the

vapor source furnace; 2) electron multiplier signal shape and dead-time losses from pulse counting; and 3) general instability in the ion source and ion counting electronics.

From the range of values listed in table 1 the multicell KEMS instrument used in this study does not maintain constant instrument sensitivity between experiments. (This is probably due to the need to turn off the ion source and open it to atmosphere when changing samples.) The small uncertainty in the 2nd law values and figure 2(a), however, suggest that S_{Au} is consistent during each experiment. Dead-time losses are only observed at the highest count rates and therefore cannot explain the higher then expected p(Au) observed below T_{mp}(Au) in figure 3(b). In any case, the dead-time, τ, of the multicell KEMS instrument was periodically determined ($\tau = 180 \pm 20$ ns) by measuring the isotopic abundance ratios of Ne, Xe, and Cr over a wide range of count rates using the method described in reference [LEO1994]. This dead-time is unusually large and probably an artifact of the shape of the peak produced by the electron multiplier. Regardless the measured τ was used to correct any counting looses and therefore is not expected to influence the results reported in this study. Thermal expansion of the multicell vapor source furnace means the distance between the effusion orifice and the first molecular beam-defining aperture, H_1, (~15 mm for the instrument used in this study) would decrease with increasing T. According to Chatillon *et al.*, [CHA1997] it is critical that the H_1 distance remains constant both within an experiment and between multiple experiments. For the furnace and T range used in this study the variation in H_1 could be as large as 0.5 mm, which could introduce a T dependence in S_{Au} that is unrelated to the evaporation behavior under investigation. Intuitively thermal expansion should act to increase S_{Au} with T, therefore assuming a fixed S_{Au} or using a value determined at a lower T will make the measured p(i) at appear to be larger then they actually are at higher T. This does not agree with the behavior observed in this study. To date there has been no effort to measure and actively maintain a constant H_1 and effectively correct for the effect of thermal expansion on observed relative partial pressure. This capability needs to be developed in future generations of the multicell KEMS instrument.

The underlying issue limiting a deeper understanding of the causes for this 5 $kJmol^{-1}$ discrepancy is in both approaches the instrument sensitivity is not truly determined independently of the evaporation behavior. The traditional approach to determining independent S_i values is to determine p(i) using the Hertz-Knudsen by measuring the mass loss of the sample plus effusion cell after a given time, Δt, at temperature T [DRO2005]. This type of calibration is not practical for these measurements because of the large number of temperature steps considered in each experiment and there is interaction between the outer surface of the graphite effusion-cell and Mo envelop. Further, as seen in reference [PAU1970a] the uncertainty with this type of calibration is of similar magnitude to the effect under investigation and therefore cannot provide a significant insight. Ideally, as suggested by Drowart *et al.*, [DRO2005], a multicell KEMS instrument needs to be developed that is capable of simultaneously measuring both the instantaneous ion intensity, I_i, and effusion flux, or absolute p(i), for a molecular beam originating from a single effusion cell over a range of temperatures. There is an initial report of the successful development of an instrument capable of simultaneously measuring the mass-loss of the effusion cell using an electronic microbalance and mass spectrometric ion intensity of the effusing molecular beam [KEM1985], but there were no subsequent publications. An approach with the potential for more success would be to combine the target-collection method [CAT1970] with multicell KEMS. In this case the instantaneous flux in the molecular beam defined by the fixed apertures of the multicell KEMS vapor source would be determined from the measure mass-gain of a target attached to an electronic microbalance mounted above the ion source of the mass spectrometer. The ability to compare the instantaneous ion intensity and effusion flux of a single molecular beam during an experiment should ultimately allow more accurate instrument sensitivities to be determined and also allow the effects of thermal expansion of the multicell vapor source furnace to be investigated.

Another aspect critical to this study is the Au–C phase diagram, particularly the solubility limit of C in liquid Au and the nature of the {Au(s) + Au(l) + Au(g) + graphite} invariant. According to current Au–C phase diagram [OKA1984] the invariant is a eutectic reaction Au(l) = Au(s) + graphite, where liquid and solid Au are expected to dissolve about 4.7at% and 0.082at%C, respectively and T_e is approximately 1323 K (T_e is not explicitly stated and the value is taken from figure 1 in [OKA1984]). The saturation limit of C in liquid Au in equilibrium with graphite is surprisingly high. If correct, there should be an observable reduction of p(Au) in equilibrium with {Au(l) + graphite} relative that in equilibrium with "pure-Au(l)". This appears to disagree with the current results that suggest p(Au) in equilibrium with {Au(s,l) + graphite} should be increased, but it is worth noting that graphite effusion-cells were used by most laboratories participating in the study discussed in reference [PAU1970a]. Therefore this original study, in general, also considered the {Au(s,l) + graphite} equilibrium not pure-Au as suggested. One laboratory (9) in that study did use Al_2O_3 lined Ir effusion-cells and their measured p(Au) was consistently higher then the accepted behavior. It would be informative to directly compare the evaporation behavior of Au in a graphite {Au(s,l) + graphite} and Al_2O_3 {Au(s,l) + Al_2O_3} effusion-cells. In theory this measurement could show the effect of C dissolution. In addition to the evaporation studies, graphite was also used to successfully contain solid and liquid Au

during heat capacity, C_p, measurements [TES1968]. The Gibbs free energy functions derived from these C_p measurements therefore should correspond to solid and liquid Au saturated with C not pure-Au. This would suggest that there is effectively no error in the reported Gibbs free energy functions of Au for this study. It would also be interesting to remeasure the C_p of Au and compare the effect of a graphite and Al_2O_3 container.

The most uncomfortable issue raised by the Au–C phase diagram is which invariant reaction are we currently using for the Au fixed point that defines ITS-90, Au(l) = Au(s) (T_{mp}(Au) = 1337.33K) or Au(l) = Au(s) + (C) (T_e~1323K). As graphite has always been used as a container for Au melting point black body sources [McG1990, FIS1989] by default we must be using the eutectic reaction in the Au–C system not the melting reaction in the Au unary system. Taking a positive view of this ambiguous situation, we could assume that T_e is equal to 1337.33K, while the actual value of T_{mp}(Au) has not being accurately determined. Given the critical importance of this fixed point it is surprising that this issue has not being properly addressed by either the metrological, materials science or thermodynamic research communities. While this study has identified the deficiencies in our knowledge of the Au–C system similar questions can be raised about the Ag–C and Cu–C systems, but in these systems the invariant is a peritectic reaction. This oversight appears to be in the process of being fixed as a number of national standards laboratories (*i.e.*, NPL, NMIJ, NIST) are currently collaborating in characterizing the temperature of a series of M(C)–C eutectic fixed points over the temperature range 1425–2750 K for a new international temperature scale [WOO2006]. From the author's perspective the scope of the investigation of M(C)–C eutectics needs to be increased beyond the characterization of the invariant temperatures to also include the investigations into the relevant phase boundaries; thermodynamic properties of the phases; and the partial pressures in the equilibrium vapor phases in the vicinity of the invariant reaction. Also as part of this broader study the Au–C, Ag–C and Cu–C systems need to be reinvestigated.

4. Conclusions

Repeated measurements (25 experiments) of the enthalpy of evaporation of {Au(s,l) + graphite}, ΔH_{sub}(298)Au, by the 2nd and 3rd law methods gave 362.2±3.3 kJmol^{-1} and 367.8±1.1 kJmol^{-1}, respectively. This ~5 kJmol^{-1} discrepancy is unacceptable for activity measurements and was removed by accepting the reproducible 2nd law ΔH_{sub}(298)Au value, which increases p(Au) by about 50%, brings the 2nd and 3rd law values into agreement and removes the T dependence in the 3rd law values. This suggests that the accepted p(Au) in equilibrium with {Au(s,l) + graphite} needs to be increased by about 50%. While these results are compelling some uncertainty remains because there is no practical method to independently determine instrument sensitivities over a range of temperatures with current multicell KEMS instruments. Therefore a new multicell KEMS instrument needs to be developed that incorporates a target-collector mounted on an electronic microbalance to allow the simultaneous determination of ion intensity and effusion flux of a single molecular beam during an experiment. This configuration should provide more accurate instrument sensitivities and also allow the effect of thermal expansion of the multicell vapor source furnace to be investigated. In addition, this study also raises a number of questions about our knowledge of the Au–C system. The Au–C phase diagram suggests a eutectic invariant reaction: L-Au(4.7at%C) = *FCC*-Au(0.08at%C) + C(graphite) at T_e~1323K. This high C concentration in Au(l) should act to reduce p(Au) in equilibrium with {Au(s,l) + graphite} and raises some critical questions about the Au fixed point that defines ITS-90. There is a critical need to reinvestigate the Au–C system.

References

ING1959 M. Inghram, J. Drowart, In High Temperature Technology, (1959) McGraw-Hill, New York, 219.

DRO2005 J. Drowart, C. Chatillon, J. Hastie, D. Bonnell, *Pure and Applied Chemistry*, 77(4), (2005), 683.

COP2007 E. Copland, *Acta Materialia*, 55 (2007), 4853–4865.

SAU1998 N. Saunders, A. Miodownik, CALPHAD: A Comprehensive Guide, Elservier Science, New York, 1998.

LEW1961 G. N. Lewis, M. Randall, Thermodynamics (revised by K. S. Pitzer and L. Brewer) McGraw-Hill, New-York, 1961, 242–278.

LUP1983 C. H. P. Lupis, Chemical Thermodynamics of Materials, North-Holland, New York, 1983. 97–112.

HIL1996 J. Kapala, D. Kath, K. Hilpert, Metall. Mater. Trans. 27A, (1996), 2673.

BUC1966 A. Büchler, J. Stauffer: in Thermodynamics (IAEA Vienna, 1966) vol. 1, 271.

CHA1974 C. Chatillion, C. Senillou, M. Allibert, A. Pattoret, *Rev. Sci. Instrum.*, 1976, 47(3), 334.

CHA1997 P. Morland, C. Chatillion, P. Rocabois, *High Temp. and Materials Sci.*, 1997, 37, 167.

CHA2002 C. Chatillion, L. Malheiros, P. Rocabois, M. Jeymond, *High Temp. High Pressures*, 2002, 34, 213.

COP2005 E. Copland, Thermodynamic Effect of Platinum Addition to β-NiAl: An Initial Investigation, NASA/CR—2005-213330, NASA, Cleveland, OH, 2005.

McG1990 M. McGlashan, *J. Chem. Thermodynamics*, 1990, 22, 653–663. (ITS–90).

PAU1970a R. C. Paule, J. Mandel, National Bureau of Standards Special Publication 260–19, 1970. Also published as: R. C. Paule, J. Mandel, *Pure and Applied Chem.*, 1972, 31, 371.

PAU1970b R. C. Paule, J. Mandel, *Pure and Applied Chem.*, 1972, 31, 395.

COP2006 E. Copland, *J. Phase Equilibrium and Diffusion*, 28(1) (2007) 38.

FIS1989 J. Fischer, H. Jung, Metrologia, 26, (1989), 245–252.

CHA1998 NIST-JANAF Thermochemical Tables, 4th Ed., American Chemical Society, 1998.

GUR1993 L. Gurvich, V. Iorish, D. Chekhovskoi, V. Yungman, IVTANTHERMO-Thermodynamic Database, Thermocenter of the Russian Academy of Sciences, Begell House 1993.

GUR1996 L. V. Gurvich, I. V. Veyts, C. B. Alcock: Thermodynamic Properties of Individual Substances, English Version, Begell House, 1996, pp. 113–208.

HOR1966 W. Horton, *J. Res. of the National Bureau of Standards A*, 70A(6), (1966), 533.

CUB1966 D. Cubicciotti, *J. Phys. Chem.*, 70(7), (1966), 2410.

PRE1990 H. Preston-Thomas, *Metrologia*, 27, (1990), 3.

OKA1984 H Okamoto, T. Massalski, *Bull. Alloy Phase Diagrams*, 5(4), (1984) and Phase Diagrams of Binary Gold Alloys, ASM International (1987).

LEO1994 W. Leo, Techniques for Nuclear and Particle Physics Experiments 2nd Edition, Springer-Verlag, New York, 1994, 122–126.

KEM1985 R. Kematick, J. Anderegg, H. Franzen, *High Temperature Science*, 19, (1985), 17–27.

CAT1970 D. Cater, Physicochemical Measurements in Metals Research, Part 1, Ed R. Rapp, Interscience Publishers, New York, (1970), Chapter 2, 21–161.

TES1968 J. Tester, R. Feber, C. Herrick, *Journal of Chemical and Engineering Data*, 13(3), (1968), 419.

WOO2006 E. Woolliams, G. Machin, D. Lowe, R. Winkler, Metrologia, 43, (2006), R11-25.

Appendix

Table A1.—Gibbs Free Energy Function, $-\left(G_T^o - H_{298}^o\right)/T$, of Au(c,l) and Au(g)

T (K)	Condensed Phase ($Jmol^{-1}K^{-1}$)	Vapor Phase ($Jmol^{-1}K^{-1}$)
298.15	47.400	180.396
900	58.703	189.461
1000	60.633	190.962
1100	62.473	192.38
1200	64.229	193.719
1300	65.909	194.986
1337.33	66.519	195.442
1400	67.935	196.187
1500	70.083	197.328
1600	72.099	198.413
1700	73.999	199.448
1800	75.795	200.438
1900	77.497	201.387
2000	79.115	202.299

These Gibbs free energy function values listed in table A1 were determined by refitting a function of the form used in [GUR1993] to the data listed in [PAU1970] and the tables produced by [GUR1993]. The functions produced by [GUR1993] could were not used because they did not reproduce the data reported in the tables.

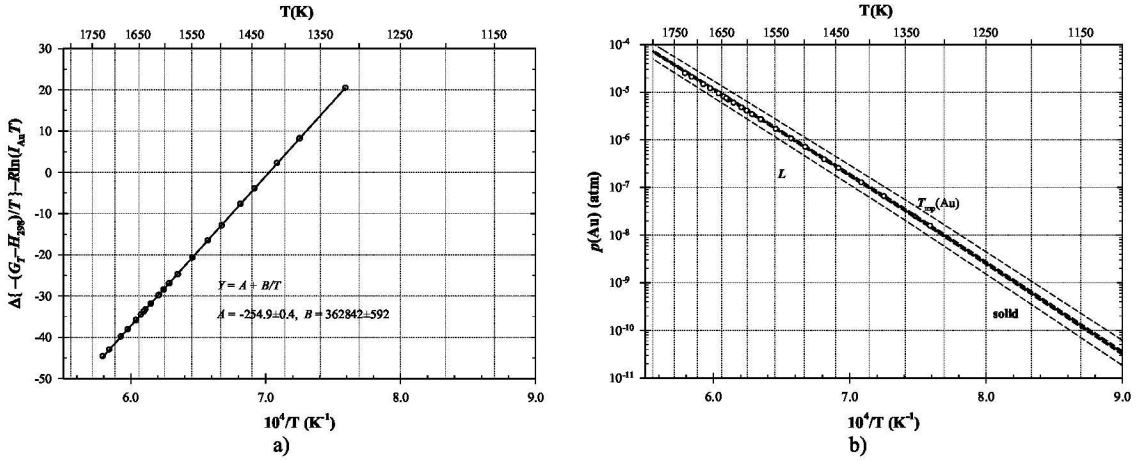

Figure A1.—Evaporation behavior of {Au(s,l) + graphite} determined during run 1. a) Second law determination of $\Delta H_{sub}(298.15)Au$ (= 362.8±0.6 kJmol^{-1}) from least squares fit of $\Delta\{-(G^{o}_{T}-H^{o}_{298})/T\}$-$R\ln(I_{Au}T)$ vs. $1/T$. b) Measured p(Au) vs. $1/T$ compared to accepted evaporation behavior found in references PAU1970 and GUR1993. In addition to the central prediction (solid line) of the evaporation behavior of Au(s,l) for $\Delta H_{sub}(298.15)Au$ = 367.0 kJmol^{-1}, this plot also shows the 95% confidence bands at the ±0.9 kJmol^{-1} and ±5.6 kJmol^{-1} levels (dashed lines).

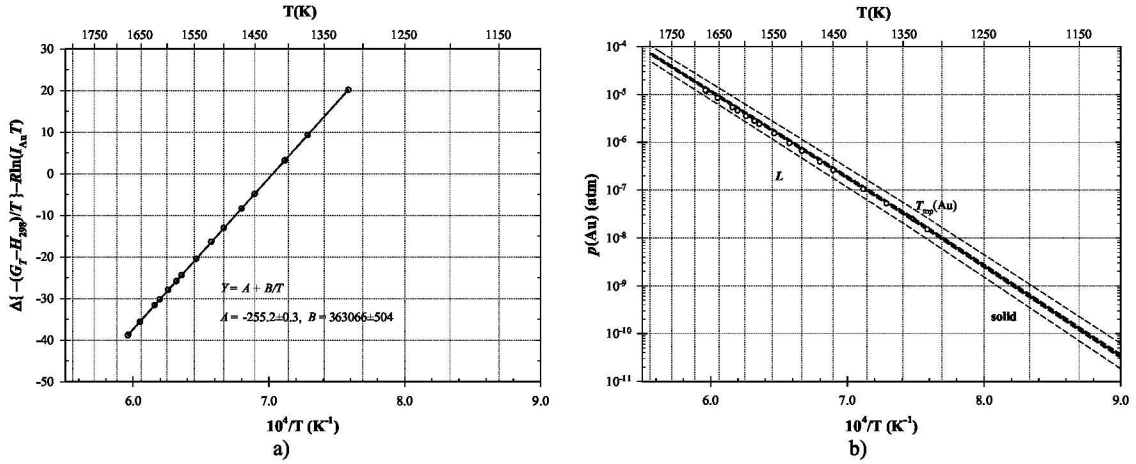

Figure A2.—Evaporation behavior of {Au(s,l) + graphite} determined during run 2. a) Second law determination of $\Delta H_{sub}(298.15)Au$ (= 363.1±0.5 kJmol^{-1}) from least squares fit of $\Delta\{-(G^{o}_{T}-H^{o}_{298})/T\}$-$R\ln(I_{Au}T)$ vs. $1/T$. b) Measured p(Au) vs. $1/T$ compared to accepted evaporation behavior found in references PAU1970 and GUR1993. In addition to the central prediction (solid line) of the evaporation behavior of Au(s,l) for $\Delta H_{sub}(298.15)Au$ = 367.0 kJmol^{-1}, this plot also shows the 95% confidence bands at the ±0.9 kJmol^{-1} and ±5.6 kJmol^{-1} levels (dashed lines).

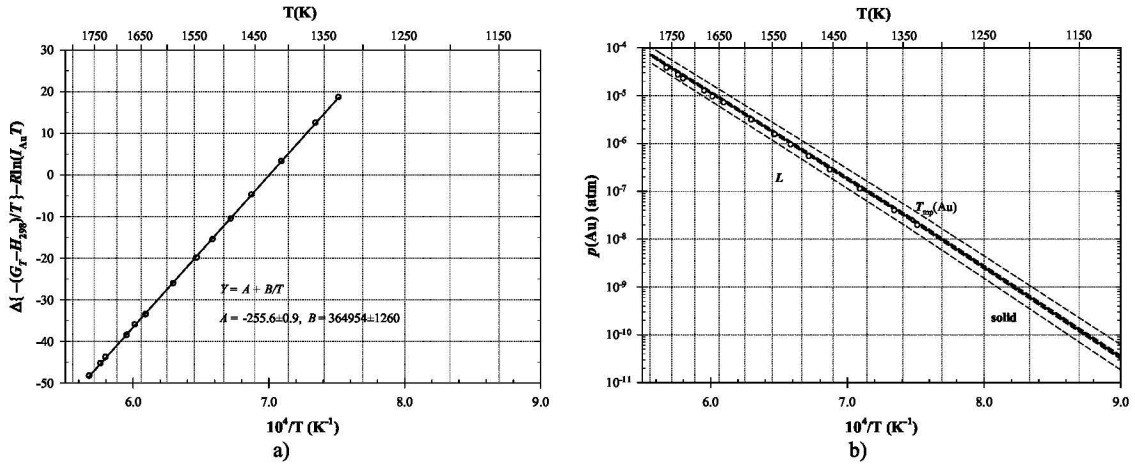

Figure A3.—Evaporation behavior of {Au(s,l) + graphite} determined during run 3. a) Second law determination of $\Delta H_{sub}(298.15)Au$ (= 364.9±1.3 kJmol^{-1}) from least squares fit of $\Delta\{-(G°_T-H°_{298})/T\}-R\ln(I_{Au}T)$ vs. $1/T$. b) Measured p(Au) vs. $1/T$ compared to accepted evaporation behavior found in references PAU1970 and GUR1993. In addition to the central prediction (solid line) of the evaporation behavior of Au(s,l) for $\Delta H_{sub}(298.15)Au$ = 367.0 kJmol^{-1}, this plot also shows the 95% confidence bands at the ±0.9 kJmol^{-1} and ±5.6 kJmol^{-1} levels (dashed lines).

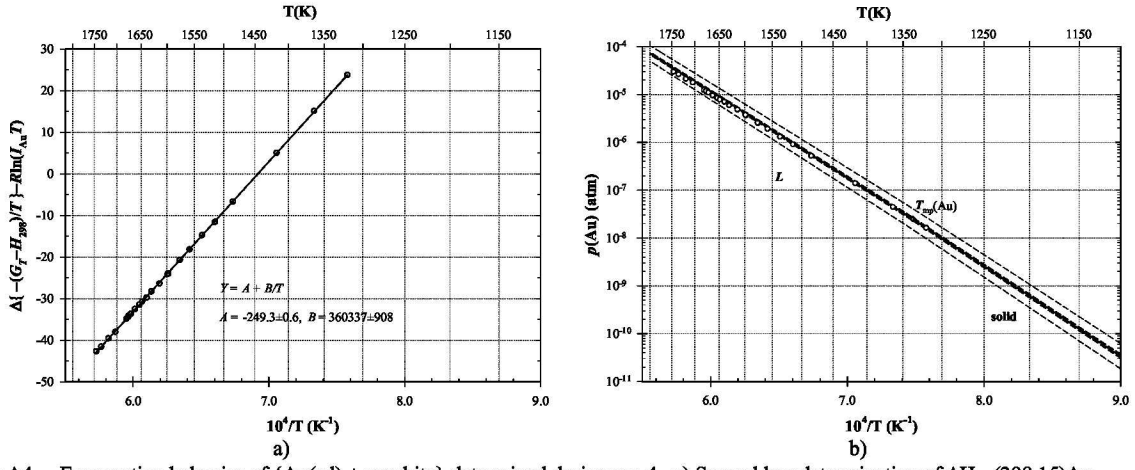

Figure A4.—Evaporation behavior of {Au(s,l) + graphite} determined during run 4. a) Second law determination of $\Delta H_{sub}(298.15)Au$ (= 360.3±0.9 kJmol^{-1}) from least squares fit of $\Delta\{-(G°_T-H°_{298})/T\}-R\ln(I_{Au}T)$ vs. $1/T$. b) Measured p(Au) vs. $1/T$ compared to accepted evaporation behavior found in references PAU1970 and GUR1993. In addition to the central prediction (solid line) of the evaporation behavior of Au(s,l) for $\Delta H_{sub}(298.15)Au$ = 367.0 kJmol^{-1}, this plot also shows the 95% confidence bands at the ±0.9 kJmol^{-1} and ±5.6 kJmol^{-1} levels (dashed lines).

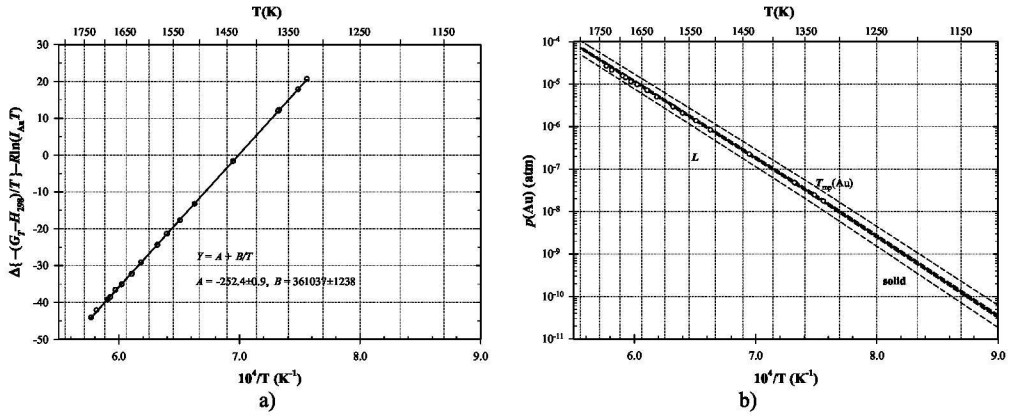

Figure A5.—Evaporation behavior of {Au(s,l) + graphite} determined during run 5. a) Second law determination of $\Delta H_{sub}(298.15)Au$ (= 361.0±1.3 kJmol^{-1}) from least squares fit of $\Delta\{-(G°_T-H°_{298})/T\}-R\ln(I_{Au}T)$ vs. $1/T$. b) Measured p(Au) vs. $1/T$ compared to accepted evaporation behavior found in references PAU1970 and GUR1993. In addition to the central prediction (solid line) of the evaporation behavior of Au(s,l) for $\Delta H_{sub}(298.15)Au$ = 367.0 kJmol^{-1}, this plot also shows the 95% confidence bands at the ±0.9 kJmol^{-1} and ±5.6 kJmol^{-1} levels (dashed lines).

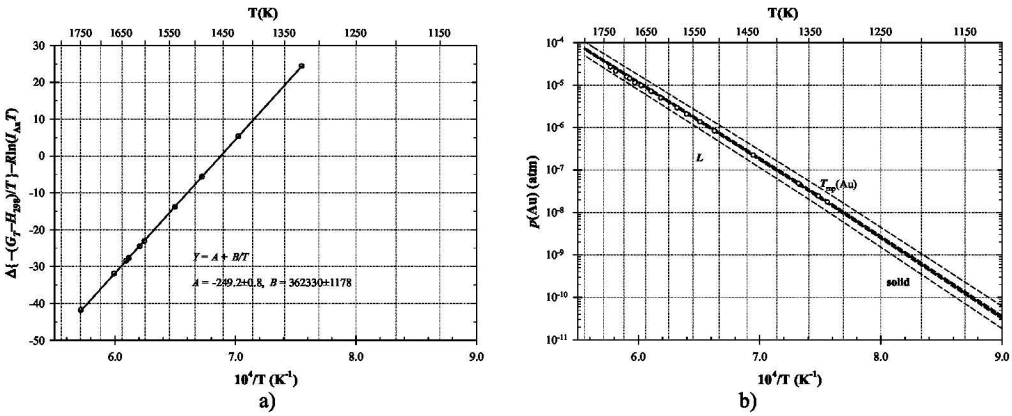

Figure A6.—Evaporation behavior of {Au(s,l) + graphite} determined during run 6. a) Second law determination of $\Delta H_{sub}(298.15)Au$ (= 362.3±1.2 kJmol^{-1}) from least squares fit of $\Delta\{-(G°_T-H°_{298})/T\}-R\ln(I_{Au}T)$ vs. $1/T$. b) Measured p(Au) vs. $1/T$ compared to accepted evaporation behavior found in references PAU1970 and GUR1993. In addition to the central prediction (solid line) of the evaporation behavior of Au(s,l) for $\Delta H_{sub}(298.15)Au$ = 367.0 kJmol^{-1}, this plot also shows the 95% confidence bands at the ±0.9 kJmol^{-1} and ±5.6 kJmol^{-1} levels (dashed lines).

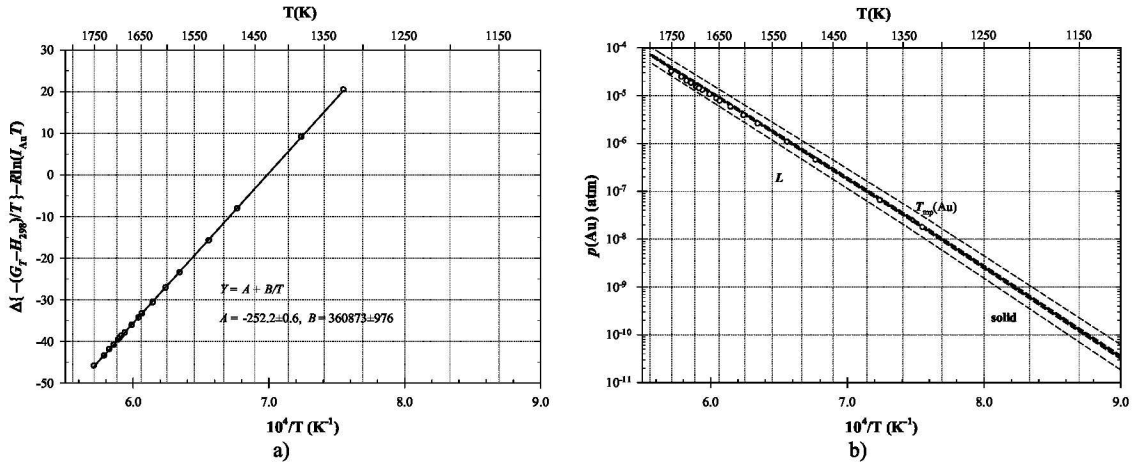

Figure A7.—Evaporation behavior of {Au(s,l) + graphite} determined during run 7. a) Second law determination of $\Delta H_{sub}(298.15)Au$ (= 360.9±1.0 kJmol^{-1}) from least squares fit of $\Delta\{-(G°_T-H°_{298})/T\}$-$R\ln(I_{Au}T)$ vs. $1/T$. b) Measured p(Au) vs. $1/T$ compared to accepted evaporation behavior found in references PAU1970 and GUR1993. In addition to the central prediction (solid line) of the evaporation behavior of Au(s,l) for $\Delta H_{sub}(298.15)Au$ = 367.0 kJmol^{-1}, this plot also shows the 95% confidence bands at the ±0.9 kJmol^{-1} and ±5.6 kJmol^{-1} levels (dashed lines).

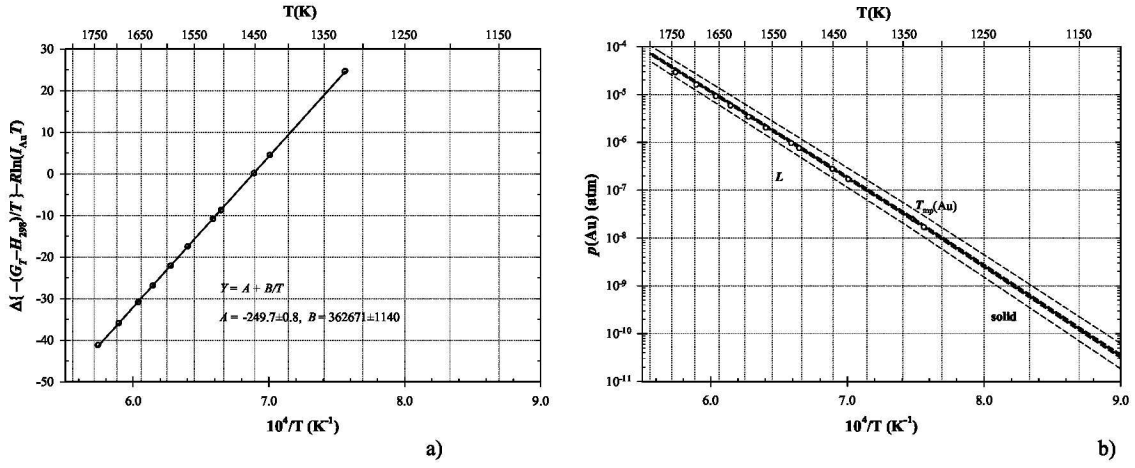

Figure A8.—Evaporation behavior of {Au(s,l) + graphite} determined during run 8. a) Second law determination of $\Delta H_{sub}(298.15)Au$ (= 362.7±1.2 kJmol^{-1}) from least squares fit of $\Delta\{-(G°_T-H°_{298})/T\}$-$R\ln(I_{Au}T)$ vs. $1/T$. b) Measured p(Au) vs. $1/T$ compared to accepted evaporation behavior found in references PAU1970 and GUR1993. In addition to the central prediction (solid line) of the evaporation behavior of Au(s,l) for $\Delta H_{sub}(298.15)Au$ = 367.0 kJmol^{-1}, this plot also shows the 95% confidence bands at the ±0.9 kJmol^{-1} and ±5.6 kJmol^{-1} levels (dashed lines).

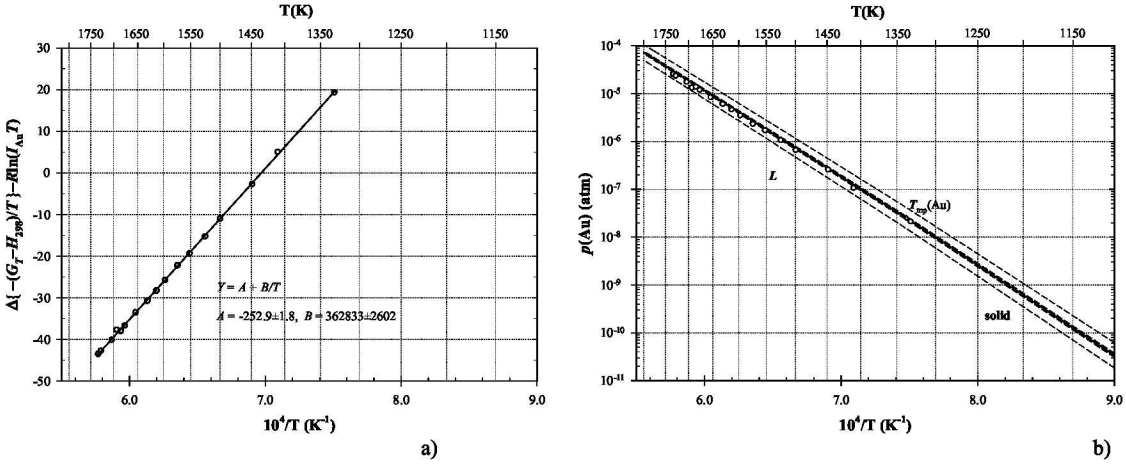

Figure A9.—Evaporation behavior of {Au(s,l) + graphite} determined during run 9. a) Second law determination of $\Delta H_{sub}(298.15)Au$ (= 362.8±2.6 kJmol^{-1}) from least squares fit of $\Delta\{-(G°_T-H°_{298})/T\}-R\ln(I_{Au}T)$ vs. $1/T$. b) Measured p(Au) vs. $1/T$ compared to accepted evaporation behavior found in references PAU1970 and GUR1993. In addition to the central prediction (solid line) of the evaporation behavior of Au(s,l) for $\Delta H_{sub}(298.15)Au$ = 367.0 kJmol^{-1}, this plot also shows the 95% confidence bands at the ±0.9 kJmol^{-1} and ±5.6 kJmol^{-1} levels (dashed lines).

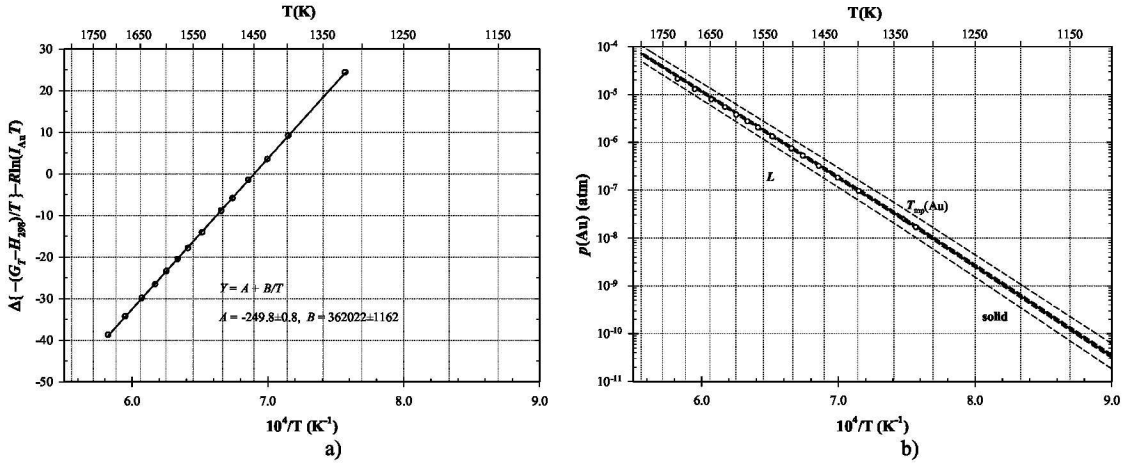

Figure A10. Evaporation behavior of {Au(s,l) + graphite} determined during run 10. a) Second law determination of $\Delta H_{sub}(298.15)Au$ (= 362.0±1.2 kJmol^{-1}) from least squares fit of $\Delta\{-(G°_T-H°_{298})/T\}-R\ln(I_{Au}T)$ vs. $1/T$. b) Measured p(Au) vs. $1/T$ compared to accepted evaporation behavior found in references PAU1970 and GUR1993. In addition to the central prediction (solid line) of the evaporation behavior of Au(s,l) for $\Delta H_{sub}(298.15)Au$ = 367.0 kJmol^{-1}, this plot also shows the 95% confidence bands at the ±0.9 kJmol^{-1} and ±5.6 kJmol^{-1} levels (dashed lines).

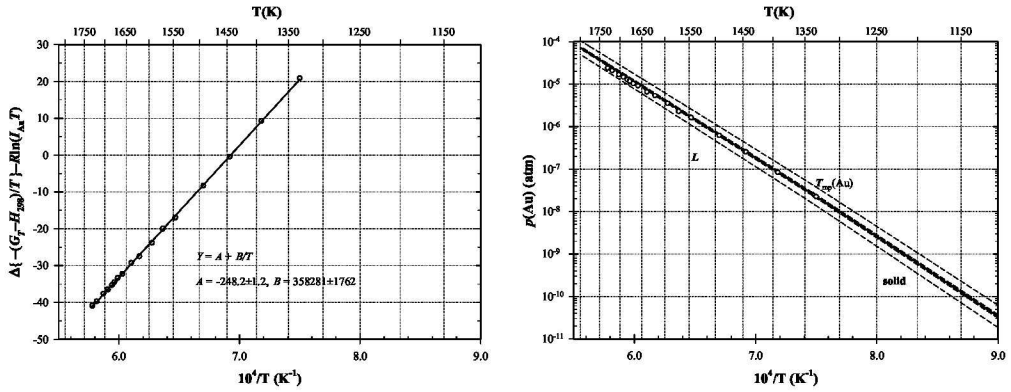

Figure A11.—Evaporation behavior of {Au(s,l) + graphite} determined during run 11. a) Second law determination of $\Delta H_{sub}(298.15)Au$ (= 358.3±1.8 kJmol^{-1}) from least squares fit of $\Delta\{-(G°_T-H°_{298})/T\}-R\ln(I_{Au}T)$ vs. $1/T$. b) Measured p(Au) vs. $1/T$ compared to accepted evaporation behavior found in references PAU1970 and GUR1993. In addition to the central prediction (solid line) of the evaporation behavior of Au(s,l) for $\Delta H_{sub}(298.15)Au$ = 367.0 kJmol^{-1}, this plot also shows the 95% confidence bands at the ±0.9 kJmol^{-1} and ±5.6 kJmol^{-1} levels (dashed lines).

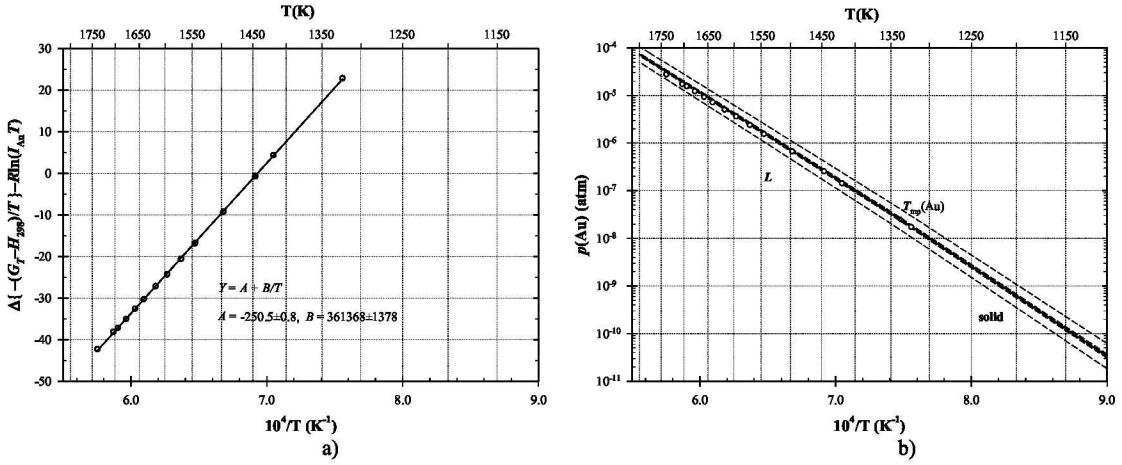

Figure A12.—Evaporation behavior of {Au(s,l) + graphite} determined during run 12. a) Second law determination of $\Delta H_{sub}(298.15)Au$ (= 361.43±1.4 kJmol^{-1}) from least squares fit of $\Delta\{-(G°_T-H°_{298})/T\}-R\ln(I_{Au}T)$ vs. $1/T$. b) Measured p(Au) vs. $1/T$ compared to accepted evaporation behavior found in references PAU1970 and GUR1993. In addition to the central prediction (solid line) of the evaporation behavior of Au(s,l) for $\Delta H_{sub}(298.15)Au$ = 367.0 kJmol^{-1}, this plot also shows the 95% confidence bands at the ±0.9 kJmol^{-1} and ±5.6 kJmol^{-1} levels (dashed lines).

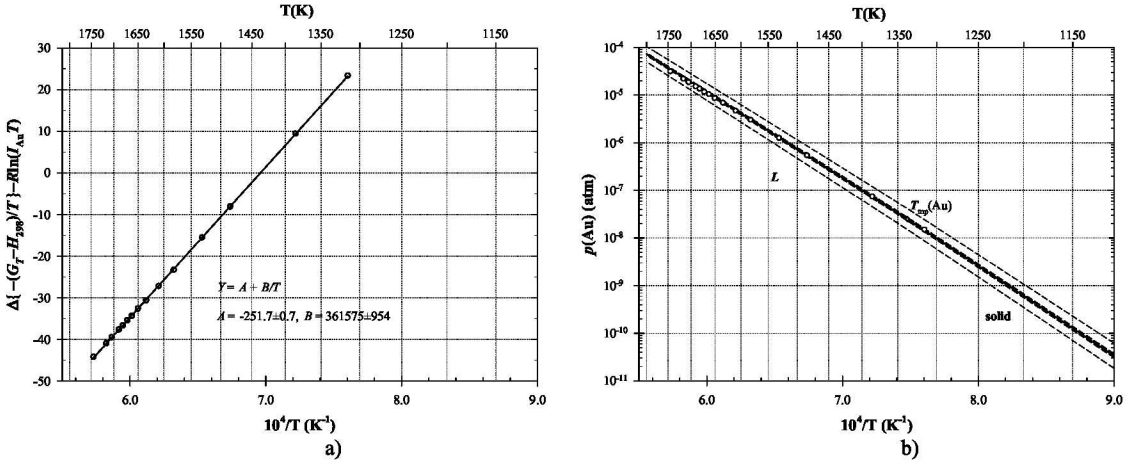

Figure A13.—Evaporation behavior of {Au(s,l) + graphite} determined during run 13. a) Second law determination of $\Delta H_{sub}(298.15)Au$ (= 361.6±0.9 kJmol^{-1}) from least squares fit of $\Delta\{-(G°_T-H°_{298})/T\}-R\ln(I_{Au}T)$ vs. $1/T$. b) Measured p(Au) vs. $1/T$ compared to accepted evaporation behavior found in references PAU1970 and GUR1993. In addition to the central prediction (solid line) of the evaporation behavior of Au(s,l) for $\Delta H_{sub}(298.15)Au$ = 367.0 kJmol^{-1}, this plot also shows the 95% confidence bands at the ±0.9 kJmol^{-1} and ±5.6 kJmol^{-1} levels (dashed lines).

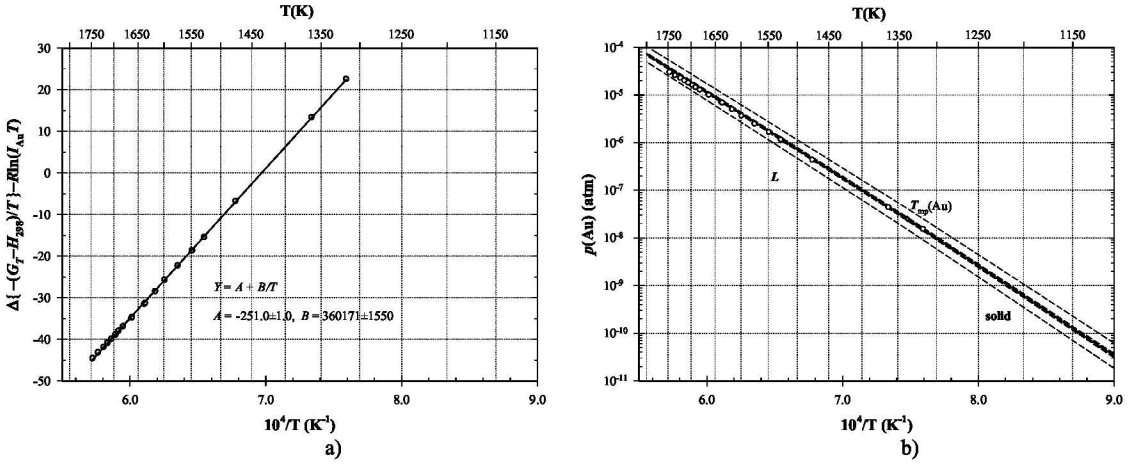

Figure A14.—Evaporation behavior of {Au(s,l) + graphite} determined during run 14. a) Second law determination of $\Delta H_{sub}(298.15)Au$ (= 360.2±1.6 kJmol^{-1}) from least squares fit of $\Delta\{-(G°_T-H°_{298})/T\}-R\ln(I_{Au}T)$ vs. $1/T$. b) Measured p(Au) vs. $1/T$ compared to accepted evaporation behavior found in references PAU1970 and GUR1993. In addition to the central prediction (solid line) of the evaporation behavior of Au(s,l) for $\Delta H_{sub}(298.15)Au$ = 367.0 kJmol^{-1}, this plot also shows the 95% confidence bands at the ±0.9 kJmol^{-1} and ±5.6 kJmol^{-1} levels (dashed lines).

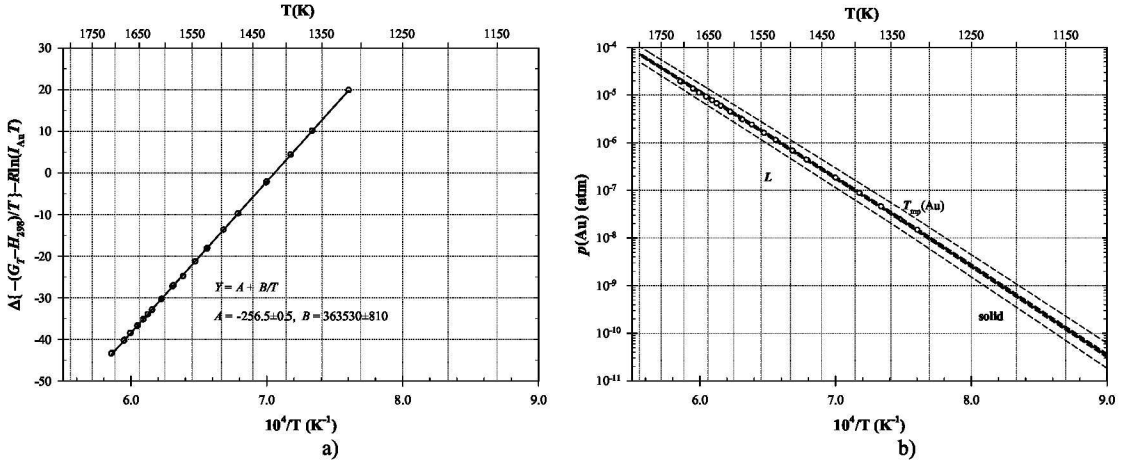

Figure A15.—Evaporation behavior of {Au(s,l) + graphite} determined during run 15. a) Second law determination of $\Delta H_{sub}(298.15)Au$ (= 363.5±0.8 kJmol^{-1}) from least squares fit of $\Delta\{-(G°_T-H°_{298})/T\}-R\ln(I_{Au}T)$ vs. $1/T$. b) Measured p(Au) vs. $1/T$ compared to accepted evaporation behavior found in references PAU1970 and GUR1993. In addition to the central prediction (solid line) of the evaporation behavior of Au(s,l) for $\Delta H_{sub}(298.15)Au$ = 367.0 kJmol^{-1}, this plot also shows the 95% confidence bands at the ±0.9 kJmol^{-1} and ±5.6 kJmol^{-1} levels (dashed lines).

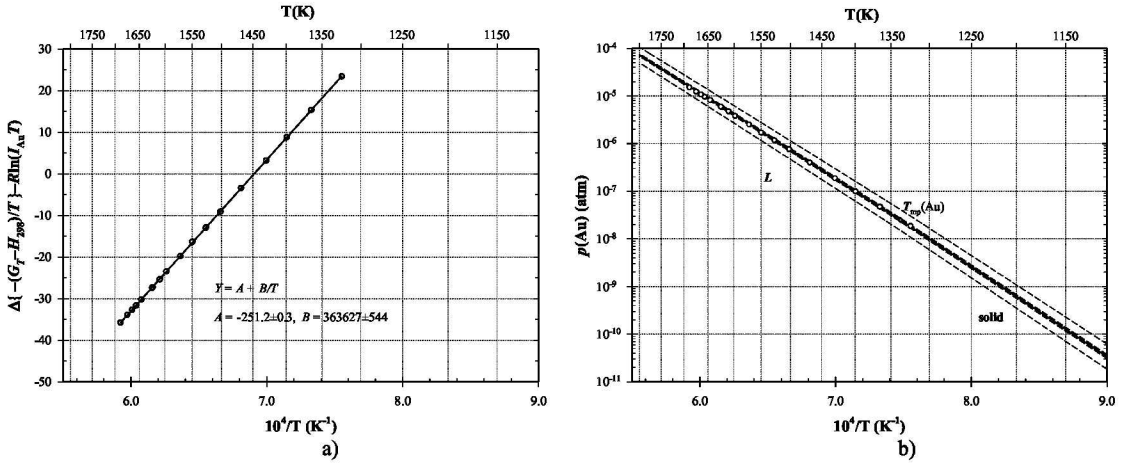

Figure A16.—Evaporation behavior of {Au(s,l) + graphite} determined during run 16. a) Second law determination of $\Delta H_{sub}(298.15)Au$ (= 363.6±0.6 kJmol^{-1}) from least squares fit of $\Delta\{-(G°_T-H°_{298})/T\}-R\ln(I_{Au}T)$ vs. $1/T$. b) Measured p(Au) vs. $1/T$ compared to accepted evaporation behavior found in references PAU1970 and GUR1993. In addition to the central prediction (solid line) of the evaporation behavior of Au(s,l) for $\Delta H_{sub}(298.15)Au$ = 367.0 kJmol^{-1}, this plot also shows the 95% confidence bands at the ±0.9 kJmol^{-1} and ±5.6 kJmol^{-1} levels (dashed lines).

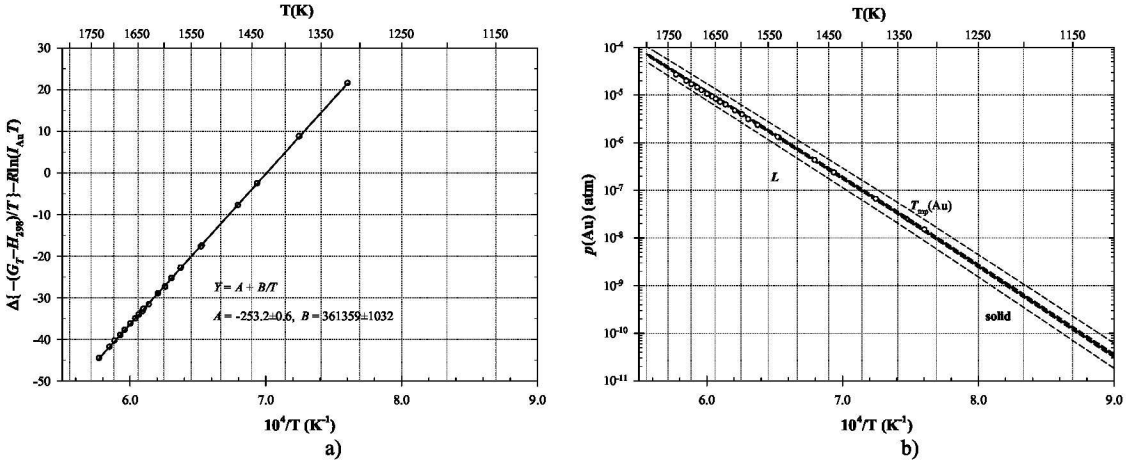

Figure A17.—Evaporation behavior of {Au(s,l) + graphite} determined during run 17. a) Second law determination of $\Delta H_{sub}(298.15)Au$ (= 361.3±1.0 kJmol^{-1}) from least squares fit of $\Delta\{-(G^{o}_{T}-H^{o}_{298})/T\}$-$R\ln(I_{Au}T)$ vs. $1/T$. b) Measured p(Au) vs. $1/T$ compared to accepted evaporation behavior found in references PAU1970 and GUR1993. In addition to the central prediction (solid line) of the evaporation behavior of Au(s,l) for $\Delta H_{sub}(298.15)Au$ = 367.0 kJmol^{-1}, this plot also shows the 95% confidence bands at the ±0.9 kJmol^{-1} and ±5.6 kJmol^{-1} levels (dashed lines).

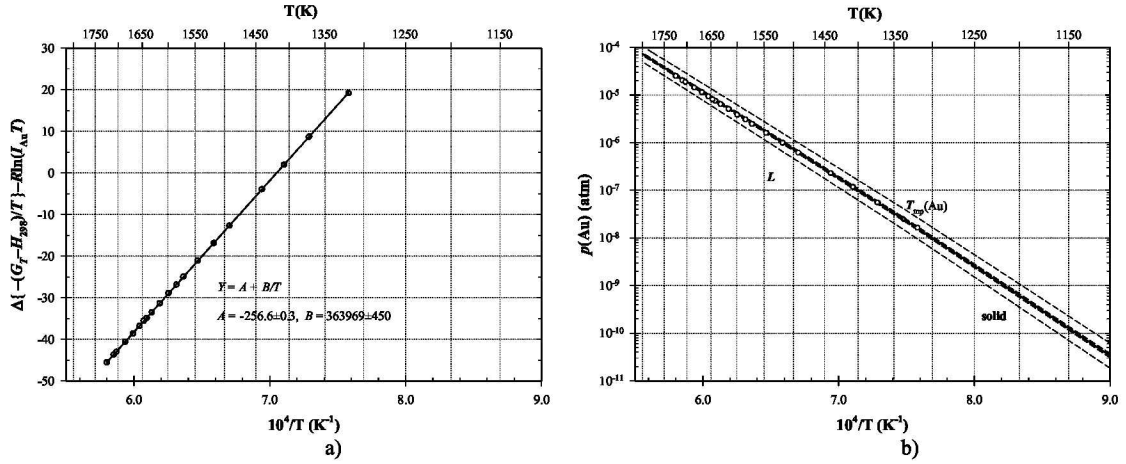

Figure A18.—Evaporation behavior of {Au(s,l) + graphite} determined during run 18. a) Second law determination of $\Delta H_{sub}(298.15)Au$ (= 364.0±0.5 kJmol^{-1}) from least squares fit of $\Delta\{-(G^{o}_{T}-H^{o}_{298})/T\}$-$R\ln(I_{Au}T)$ vs. $1/T$. b) Measured p(Au) vs. $1/T$ compared to accepted evaporation behavior found in references PAU1970 and GUR1993. In addition to the central prediction (solid line) of the evaporation behavior of Au(s,l) for $\Delta H_{sub}(298.15)Au$ = 367.0 kJmol^{-1}, this plot also shows the 95% confidence bands at the ±0.9 kJmol^{-1} and ±5.6 kJmol^{-1} levels (dashed lines).

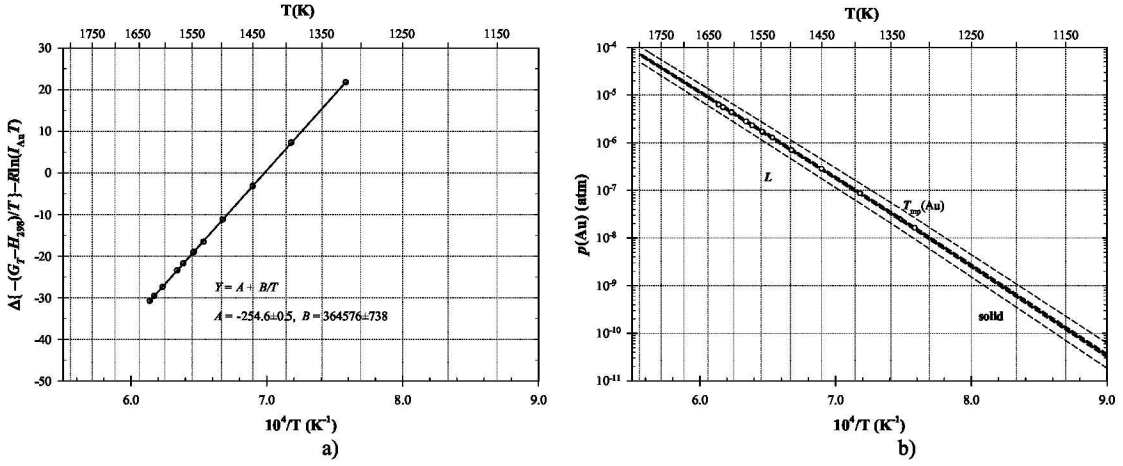

Figure A19.—Evaporation behavior of {Au(s,l) + graphite} determined during run 19. a) Second law determination of $\Delta H_{sub}(298.15)$Au (= 364.5±0.8 kJmol^{-1}) from least squares fit of $\Delta\{-(G°_T-H°_{298})/T\}-R\ln(I_{Au}T)$ vs. $1/T$. b) Measured p(Au) vs. $1/T$ compared to accepted evaporation behavior found in references PAU1970 and GUR1993. In addition to the central prediction (solid line) of the evaporation behavior of Au(s,l) for $\Delta H_{sub}(298.15)$Au = 367.0 kJmol^{-1}, this plot also shows the 95% confidence bands at the ±0.9 kJmol^{-1} and ±5.6 kJmol^{-1} levels (dashed lines).

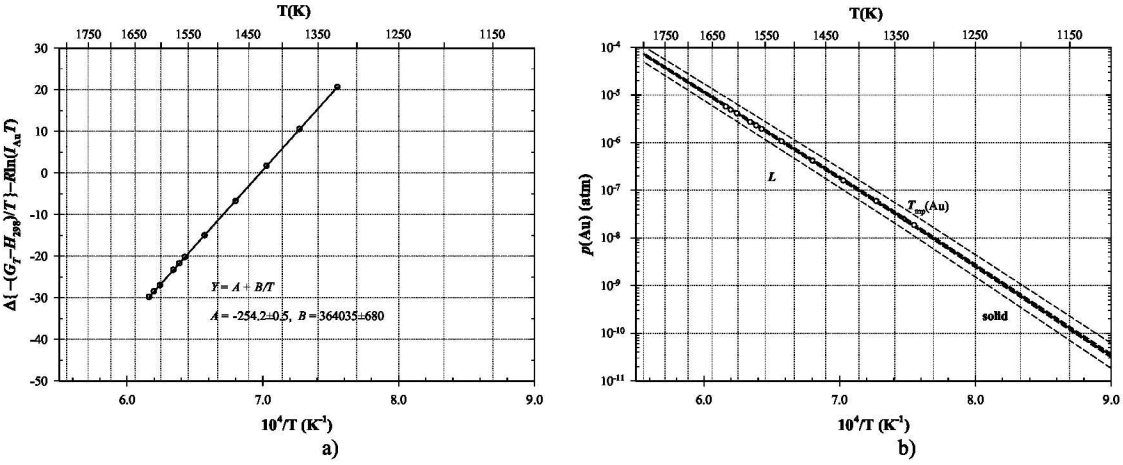

Figure A20.—Evaporation behavior of {Au(s,l) + graphite} determined during run 20. a) Second law determination of $\Delta H_{sub}(298.15)$Au (= 364.0±0.7 kJmol^{-1}) from least squares fit of $\Delta\{-(G°_T-H°_{298})/T\}-R\ln(I_{Au}T)$ vs. $1/T$. b) Measured p(Au) vs. $1/T$ compared to accepted evaporation behavior found in references PAU1970 and GUR1993. In addition to the central prediction (solid line) of the evaporation behavior of Au(s,l) for $\Delta H_{sub}(298.15)$Au = 367.0 kJmol^{-1}, this plot also shows the 95% confidence bands at the ±0.9 kJmol^{-1} and ±5.6 kJmol^{-1} levels (dashed lines).

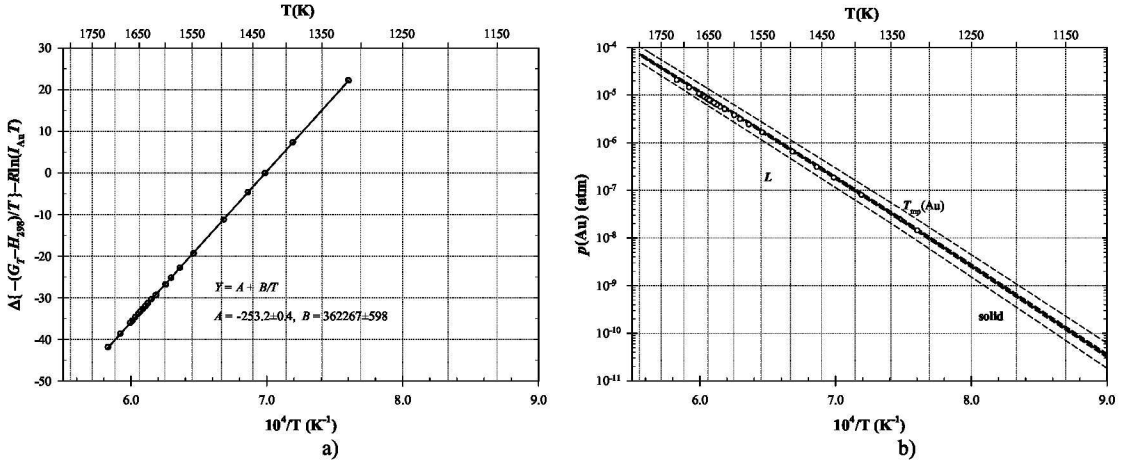

Figure A21.—Evaporation behavior of {Au(s,l) + graphite} determined during run 21. a) Second law determination of $\Delta H_{sub}(298.15)Au$ (= 362.3±0.6 kJmol^{-1}) from least squares fit of $\Delta\{-(G^{o}_{T}-H^{o}_{298})/T\}$-$R\ln(I_{Au}T)$ vs. $1/T$. b) Measured p(Au) vs. $1/T$ compared to accepted evaporation behavior found in references PAU1970 and GUR1993. In addition to the central prediction (solid line) of the evaporation behavior of Au(s,l) for $\Delta H_{sub}(298.15)Au$ = 367.0 kJmol^{-1}, this plot also shows the 95% confidence bands at the ±0.9 kJmol^{-1} and ±5.6 kJmol^{-1} levels (dashed lines).

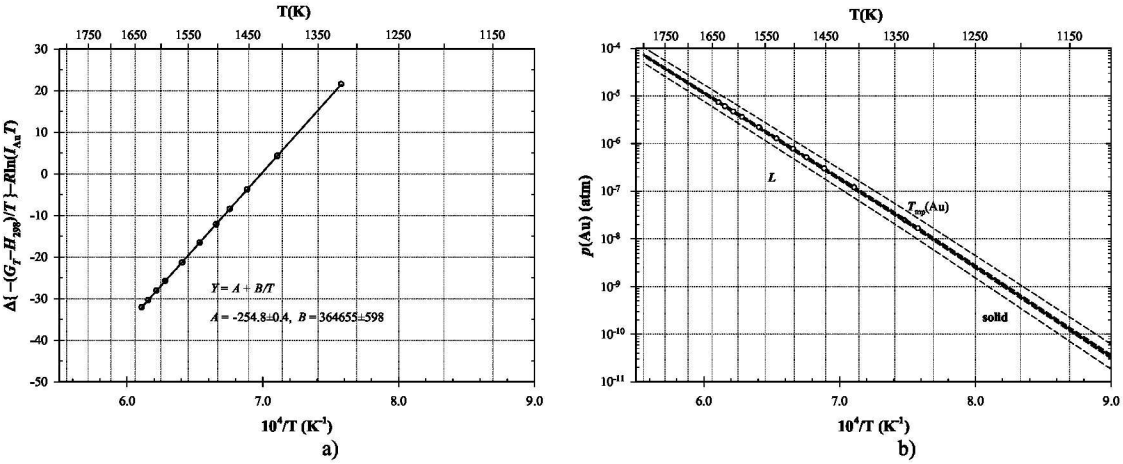

Figure A22.—Evaporation behavior of {Au(s,l) + graphite} determined during run 22. a) Second law determination of $\Delta H_{sub}(298.15)Au$ (= 364.7±0.6 kJmol^{-1}) from least squares fit of $\Delta\{-(G^{o}_{T}-H^{o}_{298})/T\}$-$R\ln(I_{Au}T)$ vs. $1/T$. b) Measured p(Au) vs. $1/T$ compared to accepted evaporation behavior found in references PAU1970 and GUR1993. In addition to the central prediction (solid line) of the evaporation behavior of Au(s,l) for $\Delta H_{sub}(298.15)Au$ = 367.0 kJmol^{-1}, this plot also shows the 95% confidence bands at the ±0.9 kJmol^{-1} and ±5.6 kJmol^{-1} levels (dashed lines).

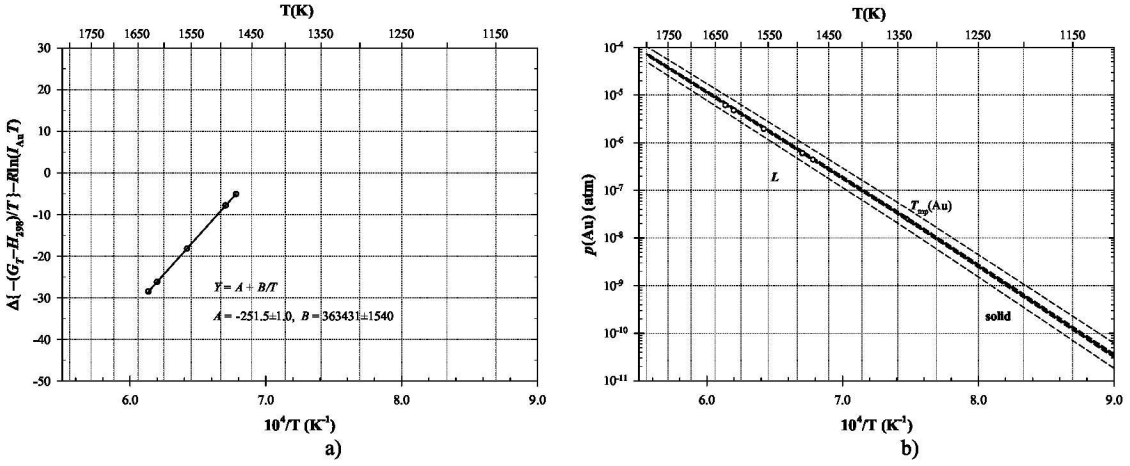

Figure A23.—Evaporation behavior of {Au(s,l) + graphite} determined during run 23. a) Second law determination of $\Delta H_{sub}(298.15)$Au (= 363.4±1.8 kJmol^{-1}) from least squares fit of $\Delta\{-(G^{\circ}_T-H^{\circ}_{298})/T\}$-$R\ln(I_{Au}T)$ vs. $1/T$. b) Measured p(Au) vs. $1/T$ compared to accepted evaporation behavior found in references PAU1970 and GUR1993. In addition to the central prediction (solid line) of the evaporation behavior of Au(s,l) for $\Delta H_{sub}(298.15)$Au = 367.0 kJmol^{-1}, this plot also shows the 95% confidence bands at the ±0.9 kJmol^{-1} and ±5.6 kJmol^{-1} levels (dashed lines).

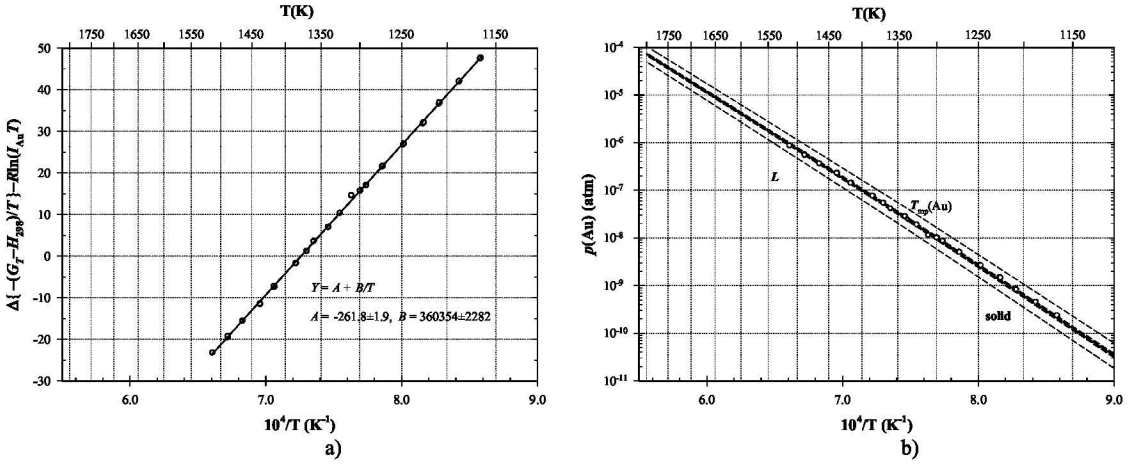

Figure A24.—Evaporation behavior of {Au(s,l) + graphite} determined during run 24. a) Second law determination of $\Delta H_{sub}(298.15)$Au (= 360.4±2.3 kJmol^{-1}) from least squares fit of $\Delta\{-(G^{\circ}_T-H^{\circ}_{298})/T\}$-$R\ln(I_{Au}T)$ vs. $1/T$. b) Measured p(Au) vs. $1/T$ compared to accepted evaporation behavior found in references PAU1970 and GUR1993. In addition to the central prediction (solid line) of the evaporation behavior of Au(s,l) for $\Delta H_{sub}(298.15)$Au = 367.0 kJmol^{-1}, this plot also shows the 95% confidence bands at the ±0.9 kJmol^{-1} and ±5.6 kJmol^{-1} levels (dashed lines).

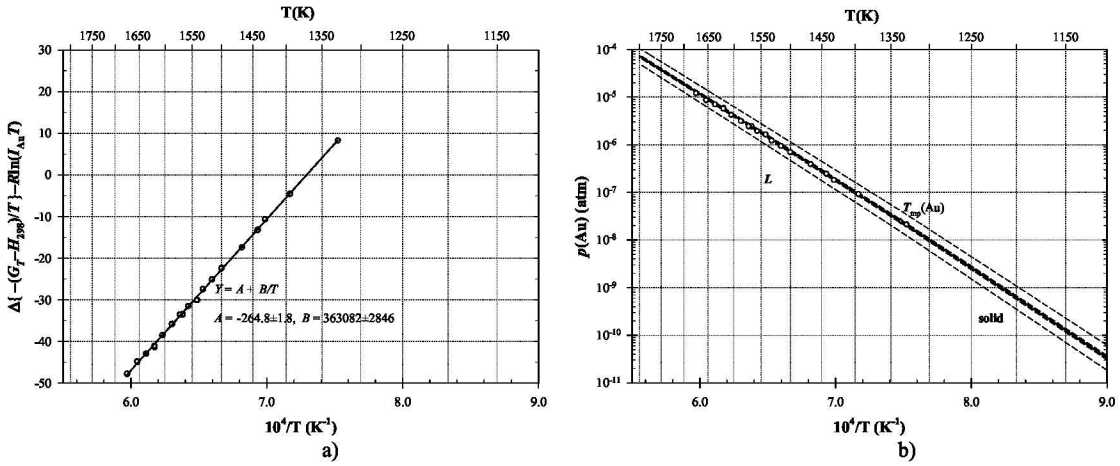

Figure A25.—Evaporation behavior of {Au(s,l) + graphite} determined during run 25. a) Second law determination of $\Delta H_{sub}(298.15)Au$ (= 363.1±2.8 kJmol^{-1}) from least squares fit of $\Delta\{-(G°_T-H°_{298})/T\}-R\ln(I_{Au}T)$ vs. $1/T$. b) Measured p(Au) vs. $1/T$ compared to accepted evaporation behavior found in references PAU1970 and GUR1993. In addition to the central prediction (solid line) of the evaporation behavior of Au(s,l) for $\Delta H_{sub}(298.15)Au$ = 367.0 kJmol^{-1}, this plot also shows the 95% confidence bands at the ±0.9 kJmol^{-1} and ±5.6 kJmol^{-1} levels (dashed lines).

REPORT DOCUMENTATION PAGE		Form Approved OMB No. 0704-0188

1. REPORT DATE *(DD-MM-YYYY)*	2. REPORT TYPE	3. DATES COVERED *(From - To)*
01-07-2009	Final Contractor Report	

4. TITLE AND SUBTITLE
Long Term Measurement of the Vapor Pressure of Gold in the Au-C System

5a. CONTRACT NUMBER
NNC07BA13B

5b. GRANT NUMBER

5c. PROGRAM ELEMENT NUMBER

6. AUTHOR(S)
Copland, Evan, H.

5d. PROJECT NUMBER

5e. TASK NUMBER

5f. WORK UNIT NUMBER
WBS 599489.02.07.03.02.04.01

7. PERFORMING ORGANIZATION NAME(S) AND ADDRESS(ES)
Case Western Reserve University
Cleveland, Ohio 44106

8. PERFORMING ORGANIZATION REPORT NUMBER
E-16808

9. SPONSORING/MONITORING AGENCY NAME(S) AND ADDRESS(ES)
National Aeronautics and Space Administration
Washington, DC 20546-0001

10. SPONSORING/MONITOR'S ACRONYM(S)
NASA

11. SPONSORING/MONITORING REPORT NUMBER
NASA/CR-2009-215498

12. DISTRIBUTION/AVAILABILITY STATEMENT
Unclassified-Unlimited
Subject Categories: 23, 25, and 34
Available electronically at http://gltrs.grc.nasa.gov
This publication is available from the NASA Center for AeroSpace Information, 443-757-5802

13. SUPPLEMENTARY NOTES

14. ABSTRACT

Incorporating the {Au(s,l) + graphite} reference in component activity measurements made with the multiple effusion-cell vapor source mass spectrometry (multicell KEMS) technique provides a fixed temperature defining ITS-90 (T_{mp}(Au) = 1337.33K) and a systematic method to check accuracy. Over a 2 year period $\Delta H_{sub}(298)$Au was determined by the 2nd and 3rd law methods in 25 separate experiments and were in the ranges 362.2±3.3 kJmol^{-1} and 367.8±1.1 kJmol^{-1}, respectively. This ~5 kJmol^{-1} discrepancy is transferred directly to the measured activities. This is unacceptable and the source of this discrepancy needs to be understood and corrected. Accepting the 2nd law value increases p(Au) by about 50 percent, brings the 2nd and 3rd law values into agreement and removes the T dependence in the 3rd law values. While compelling, there is no way to independently determine instrument sensitivities, S_{Au}, with T in a single experiment with *KEMS*. This lack of capability is stopping a deeper understanding of this problem. In addition, the Au-C phase diagram suggests a eutectic invariant reaction: L-Au(4.7at%C) = *FCC*-Au(0.08at%C) + C(graphite) at T_e ~1323K. This high C concentration in Au(l) must reduce p(Au) in equilibrium with {Au(s,l) + graphite} and raises some critical questions about the Gibbs free energy functions of Au(s,l) and the Au fixed point (T_{mp}(Au) = 1337.33K) which is always measured in graphite.

15. SUBJECT TERMS
Gold; Vaporization; Knudsen effusion mass spectrometry (KEMS); Au-C phase diagram

16. SECURITY CLASSIFICATION OF:			17. LIMITATION OF ABSTRACT	18. NUMBER OF PAGES	19a. NAME OF RESPONSIBLE PERSON
a. REPORT	b. ABSTRACT	c. THIS PAGE			STI Help Desk (email:help@sti.nasa.gov)
U	U	U	UU	29	19b. TELEPHONE NUMBER *(Include area code)* 443-757-5802